Rendiconti
Accademia Nazionale delle Scienze detta dei XL
Memorie di Scienze Fisiche e Naturali
122° (2004), Vol. XXVIII, pp. 51-88

GIULIANO FRANCESCO PANZA [1, 2] – ANTONELLA PONTEVIVO [3, *]

The Calabrian Arc: a detailed structural model of the lithosphere-asthenosphere system

Abstract – Several geodynamic processes and the lithosphere structural properties of the Central Mediterranean are still unknown and not yet completely understood. To make a step towards a better knowledge of the opening of the Tyrrhenian Basin, the subduction of the Ionian lithosphere in the Calabrian Arc and the migration of the back arc system of the Apennine chain, a fairly detailed structural model of the lithosphere-asthenosphere system (thickness, S- and P-wave velocities of the crust and of the uppermost mantle layers) has been defined for cells of 1°x1° in the Calabrian Arc region. This has been done with the non-linear inversion of local dispersion data, obtained from surface wave tomography. Available seismic and geological data derived from previous studies have been used as a priori and independent information. This study has allowed to identify a peculiar lithosphere with a very shallow Moho (less then 10 km deep) and a low V_s just below a very thin lid, in correspondence of the submarine volcanic bodies Magnaghi, Marsili and Vavilov (in the Southern Tyrrhenian Sea), whilst the lid in the area that separates Marsili from Magnaghi-Vavilov has a quite high V_s. In the areas of Aeolian islands, Vesuvius, Phlegraean Fields and Ischia a shallow and very low V_s layer in the uppermost mantle has been interpreted as their shallow-mantle magma source, while a thickened continental crust and lithospheric doubling is detected in Calabria. In the investigated part of the Ionian Sea the crust is about 25 km thick and the mantle velocity profile versus depth seems to be consistent with the presence of a continental rifted lithosphere now thermally relaxed. The resolution of our data has allowed recognizing both the subduction towards north-west of the Ionian lithosphere below the Southern Tyrrhenian Sea and the subduction of the Adriatic/Ionian lithosphere underneath the Vesuvius and Phlegraean Fields.

Key words: Surface-Wave Tomography; Non-Linear Inversion; Lithosphere-Asthenosphere System; Shallow Mantle Magma Sources; Mantle Plume; Calabrian Arc.

[1] Socio dell'Accademia. Department of Earth Sciences, University of Trieste, Via Weiss 4, I-34127 Trieste, Italy. E-mail: panza@dst.units.it

[2] The Abdus Salam International Centre for Theoretical Physics, SAND group, Trieste.

[3] Geological Institute, University of Copenhagen, Øster Voldgade 10, DK-1350 Copenhagen, Denmark. E-mail: antonella@geol.ku.dk

* Corresponding author.

Introduction

The description of the Central Mediterranean geodynamic processes and the lithosphere structural properties (for example, the nature – oceanic, continental or intermediate – of the Ionian crust) is characterised by several unknown aspects and it is still debated. In fact, the opening of the Tyrrhenian Basin, the subduction of the Ionian lithosphere in the Calabrian Arc and the migration of the back arc system of the Apennine chain, that are associated to significant lateral variations of S- (V_s) and P-wave (V_p) velocities, density (ϱ) and thickness (h) of the lithosphere, are not processes yet completely understood.

To make a step towards a better knowledge of the area of the Calabrian Arc and adjacent seas (Southern Tyrrhenian Sea, Calabria and the north-western part of the Ionian Sea; see Fig. 1), new structural models of the lithosphere-asthenosphere system (elastic properties and thickness of the crust, lid and asthenosphere) are defined for cells of 1°x1°. It is done through the non-linear inversion of local dispersion data obtained from surface wave tomography using, as a priori and independent information, available seismic and geological data derived from previous studies in these areas. The interpretation of the obtained spatial distribution versus depth of V_s is performed considering the distributions versus depth of the seismic energy release and comparing the structure of each cell in the study area with pertinent independent (geochemical and petrological) models of the lithosphere [1, 12, 33, 40, 55, 58, 65, 87, 89, 112, 136].

The primary aim of this study is to sample the depth range (Moho discontinuity-250 km) where body wave tomography does not have optimal resolution [2, 3, 5, 8, 27, 53, 74, 96, 97, 98, 109, 110, 118] as the so far performed surface wave tomography [79, 81, 82, 83, 103, 104, 113, 117].

[113] present the dispersion characteristics (in the period range 20-200 s for Rayleigh waves and 20-125 s for Love waves) of surface waves propagating across Eurasia, with average resolutions ranging from 5° to 7.5°.

The V_s velocity model of [79] is a regional European model obtained, using a partitioned waveform inversion, from waveforms in the time window starting at the V_s arrival and ending after the fundamental mode Rayleigh wave arrival. The method takes into account surface wave mode coupling but neglects the important effect of amplitude differentiation [42]. In the retrieval of their model, [79] have used three background velocity models and have demonstrated that the velocity perturbation in the upper layer (from the surface down to a depth of about 30 km) of the inverted model is a combination of the effects of using an erroneous crustal thickness in the background model and of lateral heterogeneity. For this reason they focus on the deeper part of the upper mantle, for which the influence of crustal thicknesses is small. Our surface-wave tomography study, instead, does not require resorting to any background model.

[81] and [82] propose an objective regionalization of group velocity Rayleigh wave dispersion data for the Mediterranean area. The authors use the Backus-

Gilbert formulation [6, 7] and Yanovskaya methodology [37, 129, 132] for the computation of local group velocities from path-averaged dispersion curves for periods from 10 s to 70 s. We consider both group and phase velocity dispersion curves, spanning the period range 10 - 100 s and reaching the penetration depth of about 250 km.

Furthermore, our purpose is to see if there are indications of relevant phenomena of partial melting, in the investigated depth range, more or less directly related to volcanism. Thus, the main elements that we are going to consider are: (1) the lithospheric structure in correspondence of the Marsili and Magnaghi-Vavilov huge volcanic bodies in the Tyrrhenian Sea; (2) the evaluation of the horizontal

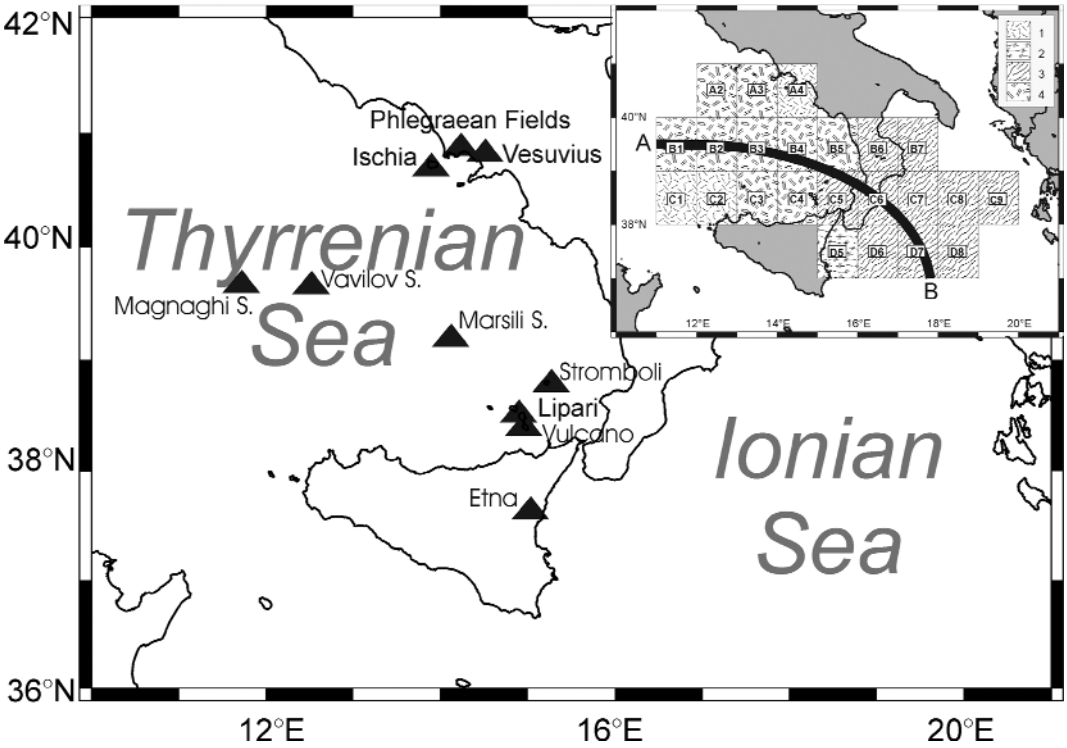

Fig. 1 - The study area and the considered cells. The recent volcanoes (INGV web page: http://www.ingv.it/vulcani/vulcani-mappa.html) in the Tyrrhenian area are plotted as triangles: Ischia (in A3), Phlegraean Fields and Vesuvius (in A4), Lipari and Vulcano (in C4), Stromboli (in C5), Etna (in D5). Magnaghi (in B1), Vavilov (in B2) and Marsili (in B4) Seamounts are also plotted. In the insert, different patterns indicate different phase (C) and group (U) velocity measurement errors associated to the cells, according to the path coverage: (1) U measurement error equal to twice ϱ_{Um} (bad coverage) and C measurement error equal to ϱ_{Cm} (good coverage); (2) measurement errors equal to twice ϱ_{Um} and twice ϱ_{Cm} (bad coverage both in group and phase velocities); (3) measurement errors equal to ϱ_{Um} and twice ϱ_{Cm} (bad coverage in phase velocity); (4) measurement errors equal to ϱ_{Um} and ϱ_{Cm} (good coverage both in group and phase velocities). The black bold line represents the study section AB following the line of the palaeogeographic prolongation of the Ionian "Ocean" towards the northwest proposed by [23].

extension, at depth, of the sub-marine volcanic bodies characterising the Southern Tyrrhenian Sea, in so far as the resolution of this tomography study allows us; (3) the presence of shallow mantle magma sources in the areas of Aeolian Islands, Vesuvio, Ischia and Phlegraean Fields; (4) the evidences about the subduction towards north-west of the Ionian lithosphere below the Southern Tyrrhenian Sea; (5) the definition of the lithospheric structure in the Ionian Sea; (6) the evidences about the subduction of the Adriatic/Ionian lithosphere.

Geological setting

The Southern Tyrrhenian Sea is a basin characterised by a thinned continental crust, about 20 km thick in periphery [72, 108], and its thickness reduces progressively to less than 10 km, going towards the basin centre.

The central crust, that is younger than 6 Ma and even younger (less than 1.9 Ma) in its eastern part, in correspondence of the Marsili Basin [43, 64], is oceanic and lies on the top of abnormal (very low V_s) mantle [72, 92]. In fact, in the central part of the basin, below the oceanic crust, there are shallow anomalous mantle materials [23, 99, 100, 120] in correspondence of the huge submarine seamounts, peculiar of the area (Marsili and Magnaghi-Vavilov). The volcanism in the Southern Tyrrhenian Sea was characterised by tholeitic magmas, similar to mid-ocean ridge magmas, which were thrown out by the mantle in Ustica between 7.5 Ma and 2.5 Ma ago [30]. Then there were also eruptions of alkali basalts and, between 1.3 Ma and 0.2 Ma ago, the volcanism moved away from the centre of the Tyrrhenian Basin becoming calc-alkaline. More recently, lavas from the potassic series (shoshonite) appeared in the Aeolian Islands (100.000 years ago in Vulcano and 30.000 years ago in Stromboli). This volcanism evolution is different from that of the «traditional» intra-arc basin and, perhaps, it is due to the contamination of the magma by continental sediments, which thicken progressively going away from the centre of the basin [72]. The extension of the volcanic bodies in the Southern Tyrrhenian Sea is not very clear but it seems to be larger than earlier believed and, in fact, [78] define the Marsili Basin to be nearly circular in shape with a diameter of the order of 120 km. The Aeolian arc is a volcanic structure extending for about 200 km along the north-western side of the Calabro-Peloritano block. The arc, for its magma composition and for the evolution of the magmatism, consists of two main sectors separated by the central islands of Vulcano and Lipari [16]: the western sector is constituted by Alicudi and Filicudi islands and by the seamounts of Sisifo, Enarete, Eolo, North Alicudi and North Filicudi; the eastern sector by Panarea and Stromboli islands and the seamount of Lamentini. Salina Island lies at the intersection between the western sector and the Lipari-Vulcano alignment. The geochemical analysis of [105] shows that the mantle sources beneath Vesuvius, Phlegraean Fields and Stromboli consists of a mixture of intraplate- and slab-derived components.

The Calabrian Arc is involved in the subduction of the Ionian lithosphere towards north-west, below the Tyrrhenian Sea, where the depth of the earthquake sources increases with increasing distance from the Calabrian Arc [4, 19, 21]. This Wadati-Benioff Zone represents an interesting object of study. From the geodynamics point of view, for example, [39, 40] propose a different degree of rollback of the oceanic side of the slab (Ionian part) with respect to the continental western counterpart (western part of Sicily), which generated a slab window along the Malta escarpment favouring mantle melting just below the Etna [58]. [94] propose a sketch representation of the geometry of the lithosphere involved in the subduction where one can identify different volumes, each one characterised by its own uniform stress distribution [15], and the existence of a window on the asthenosphere beneath northern Calabria [80], that could be related to the presence of Vulture volcano. Moreover, [56] described the western Mediterranean as a Neogene-Quaternary back-arc setting with dispersed and stretched boudins of continental lithosphere: while the eastward roll-back of the Apenninic subduction seems quite continuous, the back-arc area is instead punctuated by jumps in the spreading position. This lithosphere boudinage would confirm the presence of an underlying eastward-migrating asthenosphere [137].

The Ionian Sea, which had an important role in the interaction between Africa and Europe during Tertiary and Quaternary, represents a key area for understanding the evolution of the Mediterranean geodynamics, both for the Apennines and Hellenic subduction zones [23, 39]. There is still a debate about the evolution of the Ionian Sea and its lithospheric properties. [23], [36], [49], [75] and [119] consider the Ionian abyssal plain floored by oceanic crust, which is about 14 km thick and is covered by about 8 km of flat-lying sediments. From a review of the geophysical data of the Ionian basin, [23] propose that the Ionian Sea is an abyssal plain of oceanic nature, bounded by two conjugate passive continental margins (Apulia and Malta escarpments), and that the disappearance of the original median ridge is due to thermal cooling and lateral burial by tertiary sediments. On the other side [11], [17], [28], [44], [62], [95] and [127] propose that the Ionian basin crust is of continental-intermediate type (thinned and stretched). From the reconstruction of the palaeotectonic and palaeogeographic history of the Eastern Mediterranean area (taking into account the presence of large dinosaurs on the Apulia carbonate platform), [11] supports the hypothesis that the Ionian basin is mostly occupied by a stretched attenuated continental crust area generated during the Jurassic extensional phase. Moreover, [72] suggests that the Ionian Basin, between Sicily and Peloponnesus, is not an oceanic subducted basin below the Calabrian arc and that its bottom is a thinned continental crust (20 km thick) and the foreland of Africa.

The Method

Surface waves dispersion curves, determined along different paths by the Frequency-Time Analysis [70, 71], and tomographic methods applied to these measurements are widely used to study lateral variations of the crust and of the upper mantle [63, 81, 82, 83, 102, 111, 113, 126, 130, 131, 133, 134]. To determine the thickness and the vertical velocity distribution of the lithospheric layers in the area under investigation, represented in Fig. 1, we consider the surface-wave tomography regional study made by [111] and, where pertinent, the large-scale one by [102].

Some examples of tomography maps of group and phase velocities obtained by [111], using the two-dimensional tomography algorithm developed by [37] and [132] are shown in Fig. 2. Their lateral resolving power is of about 200 km. However, if some parameters of the uppermost part of the crust are fixed, on the base of a priori independent geological and geophysical information, the lateral resolving power may be improved and it justifies the choice to perform the inversion for cells of 1°x1°. Each cell of the grid is characterised by average dispersion curves of group velocity, U(T) (in the period range of 10-35 s), and of phase velocity, C(T) (in the period range of 25-100 s). Each mean cellular velocity is the average of the values read from the relevant tomography maps at the four knots of each 1°x1° cell. The dispersion relations computed in this way are listed in Tab.1.

At each period the measurement error for the group velocity is estimated from the difference in the group velocity values determined along similar paths crossing similar areas, and it is assumed to be the same, ϱ_{Um}, in all the cells characterised by a good path-coverage. For the cells with a low path-coverage, the assumed error is twice ϱ_{Um}. The measurement error associated to the phase velocity, ϱ_{Cm}, is fixed according to typical values given in the literature [9, 20] in cells with a good path-coverage, and it is twice ϱ_{Cm} elsewhere. In the insert of Fig. 1 the cells are grouped according to the measurement errors associated to group and phase velocities.

In the inversion, each single point error (ϱ_U, ϱ_C) associated to group and phase velocity values of a cell (listed in Tab. 1), is the 2D Euclidean norm (quadratic sum) of the measurement error (ϱ_{Um}, ϱ_{Cm}) and of the standard deviation (σ_U, σ_C) of the average cellular velocities (U(T), C(T)). In general, the latter error is negligible with respect to the former.

Non-linear Inversion

Average models of the crust and of the upper mantle are retrieved by the non-linear inversion method called Hedgehog [67, 90, 123, 124] applied to the 1°x1° averaged dispersion relations. The solutions retrieved in such a way are independent from the starting model. This inversion method represents an optimized Monte Carlo search. Following this procedure, the structure is modelled as a stack of N homogeneous isotropic elastic layers and each layer is defined by V_s, V_p, ϱ and h. Each parameter of the structure can be independent (the parameter is variable and

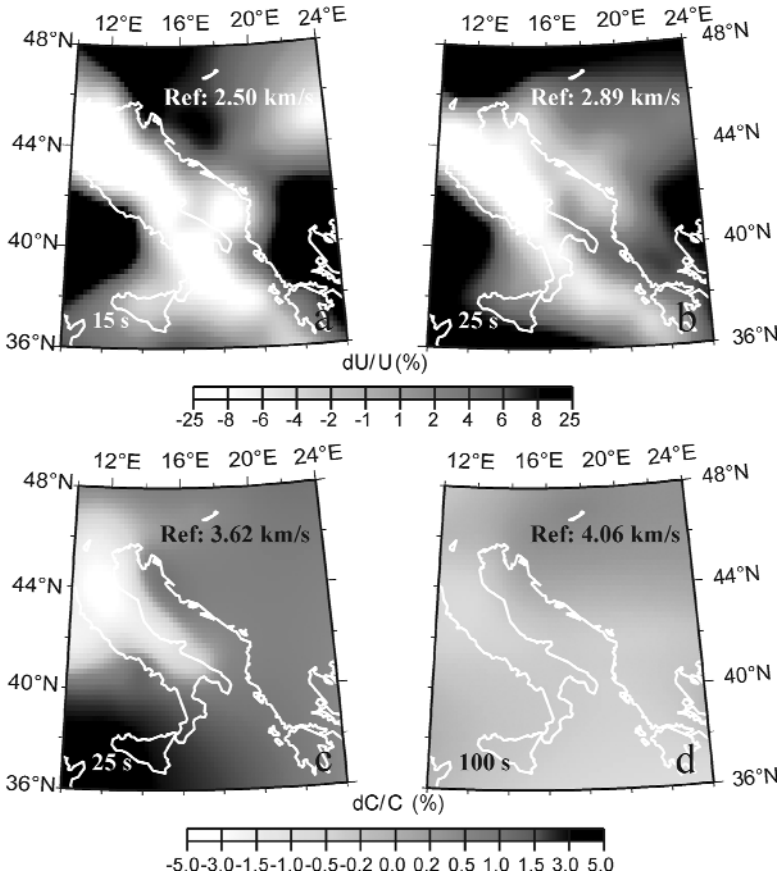

Fig. 2 - Percent variation of group, dU/U, and phase, dC/C, velocities with respect to the reference value (Ref.): group velocity tomography maps at 15 s (a) and 25 s (b) and phase velocity tomography maps at 25 s (c) and 100 s (d).

can be well resolved by the data), dependent (the parameter has a fixed relationship with an independent parameter) or fixed (the parameter is held constant during the inversion, according to independent geophysical evidences). For each structural model, phase and group velocity curves are computed and if, at each period, the difference, $\hat{d}_i$, between the computed and the experimental values is less than the single point error (ϱ_U, ϱ_C), and if the r.m.s. values (two distinct values: one for the phase and one for the group velocity) of the differences are less than a chosen fraction (usually between 60-70%) of the average of the single point errors, the model is accepted [9, 90]. Since the problem is not unique, for each cell the solution is composed by a set of models (accepted structures), which depends on the parameterization used.

Tab. 1 - Group (U) and phase (C) velocity values at different periods (from 10 s to 35 s and from 25 s to 100 s, respectively) with the single point error (ϱ_U , ϱ_C) and the r.m.s. values for each cell. All phase velocities have been corrected for sphericity following [10].

	Cell A2 (12.5; 40.5)				**Cell A3 (13.5; 40.5)**				**Cell A4 (14.5; 40.5)**				**Cell B1 (11.5; 39.5)**				**Cell B2 (12.5; 39.5)**			
T	U	ϱ_U	C	ϱ_C	U	ϱ_U	C	ϱ_C	U	ϱ_U	C	ϱ_C	U	ϱ_U	C	ϱ_C	U	ϱ_U	C	ϱ_C
(s)	(km/s)	(km/s)	(km/s)	(km/s)	(km/s)	(km/s)	(km/s)	(km/s)	(km/s)	(km/s)	(km/s)	(km/s)	(km/s)	(km/s)	(km/s)	(km/s)	(km/s)	(km/s)	(km/s)	(km/s)
10	2.60	0.1			2.55	0.11			2.36	0.2			2.51	0.1			2.53	0.1		
15	2.99	0.08			2.74	0.12			2.45	0.17			2.95	0.1			2.85	0.11		
20	3.14	0.08			2.89	0.11			2.63	0.15			3.16	0.1			3.02	0.1		
25	3.17	0.08	3.64	0.11	2.96	0.1	3.65	0.11	2.76	0.15	3.64	0.11	3.28	0.08	3.68	0.11	3.16	0.08	3.68	0.11
30	3.36	0.08	3.68	0.09	3.22	0.1	3.69	0.09	3.06	0.16	3.69	0.09	3.4	0.09	3.71	0.09	3.3	0.08	3.7	0.09
35	3.51	0.16	3.7	0.08	3.37	0.17	3.72	0.08	3.2	0.32	3.73	0.08	3.52	0.16	3.74	0.08	3.44	0.16	3.73	0.08
50			3.81	0.06			3.83	0.06			3.85	0.06			3.83	0.06			3.81	0.06
80			3.93	0.06			3.94	0.06			3.94	0.06			3.92	0.06			3.92	0.06
100			3.98	0.06			3.98	0.06			3.98	0.06			3.99	0.06			3.99	0.06
r.m.s.		0.07		0.055		0.07		0.055		0.12		0.055		0.07		0.055		0.07		0.055
	Cell B3 (13.5; 39.5)				**Cell B4 (14.5; 39.5)**				**Cell B5 (15.5; 39.5)**				**Cell B6 (16.5; 39.5)**				**Cell B7 (17.5; 39.5)**			
T	U	ϱ_U	C	ϱ_C	U	ϱ_U	C	ϱ_C	U	ϱ_U	C	ϱ_C	U	ϱ_U	C	ϱ_C	U	ϱ_U	C	ϱ_C
(s)	(km/s)	(km/s)	(km/s)	(km/s)	(km/s)	(km/s)	(km/s)	(km/s)	(km/s)	(km/s)	(km/s)	(km/s)	(km/s)	(km/s)	(km/s)	(km/s)	(km/s)	(km/s)	(km/s)	(km/s)
10	2.47	0.11			2.34	0.11			2.19	0.1			2.11	0.1			2.18	0.11		
15	2.69	0.1			2.5	0.09			2.36	0.09			2.27	0.08			2.29	0.09		
20	2.85	0.09			2.68	0.08			2.56	0.08			2.47	0.07			2.44	0.07		
25	3.02	0.08	3.68	0.11	2.89	0.08	3.67	0.11	2.78	0.08	3.66	0.11	2.73	0.07	3.65	0.22	2.80	0.09	3.65	0.22
30	3.21	0.09	3.7	0.09	3.11	0.08	3.7	0.09	3.05	0.08	3.7	0.09	3.02	0.08	3.7	0.18	3.07	0.09	3.7	0.18
35	3.36	0.16	3.73	0.08	3.28	0.16	3.74	0.08	3.24	0.16	3.75	0.08	3.25	0.16	3.75	0.16	3.32	0.16	3.75	0.16
50			3.82	0.06			3.84	0.06			3.85	0.06			3.86	0.12			3.86	0.12
80			3.93	0.06			3.93	0.06			3.92	0.06			3.92	0.12			3.92	0.12
100			3.99	0.06			3.98	0.06			3.98	0.06			3.98	0.12			3.98	0.12
r.m.s.		0.07		0.055		0.07		0.055		0.07		0.055		0.07		0.09		0.07		0.09

Tab. 1 (*segue*)

	Cell C1 (11.5; 38.5)				**Cell C2 (12.5; 38.5)**				**Cell C3 (13.5; 38.5)**				**Cell C4 (14.5; 38.5)**				**Cell C5 (15.5; 38.5)**			
T	U	ϱ_U	C	ϱ_C	U	ϱ_U	C	ϱ_C	U	ϱ_U	C	ϱ_C	U	ϱ_U	C	ϱ_C	U	ϱ_U	C	ϱ_C
(s)	(km/s)	(km/s)	(km/s)	(km/s)	(km/s)	(km/s)	(km/s)	(km/s)	(km/s)	(km/s)	(km/s)	(km/s)	(km/s)	(km/s)	(km/s)	(km/s)	(km/s)	(km/s)	(km/s)	(km/s)
10	2.44	0.2			2.41	0.2			2.34	0.11			2.25	0.11			2.16	0.1		
15	2.73	0.17			2.63	0.17			2.52	0.1			2.45	0.08			2.39	0.08		
20	2.91	0.15			2.8	0.15			2.71	0.08			2.66	0.07			2.62	0.07		
25	3.19	0.14	3.74	0.11	3.1	0.14	3.73	0.11	3.01	0.08	3.72	0.11	2.93	0.07	3.7	0.11	2.87	0.07	3.68	0.22
30	3.34	0.16	3.75	0.09	3.25	0.16	3.74	0.09	3.17	0.08	3.73	0.09	3.11	0.08	3.72	0.09	3.07	0.08	3.72	0.18
35	3.48	0.32	3.78	0.08	3.41	0.32	3.77	0.08	3.34	0.16	3.76	0.08	3.28	0.16	3.76	0.08	3.26	0.16	3.76	0.16
50			3.84	0.06			3.83	0.06			3.83	0.06			3.84	0.06			3.85	0.12
80			3.93	0.06			3.92	0.06			3.92	0.06			3.92	0.06			3.92	0.12
100			3.99	0.06			3.99	0.06			3.99	0.06			3.98	0.06			3.98	0.12
r.m.s.	0.12		0.055		0.12			0.055		0.07		0.055		0.07		0.055		0.07		0.09
	Cell C6 (16.5; 38.5)				**Cell C7 (17.5; 38.5)**				**Cell C8 (18.5; 38.5)**				**Cell C9 (19.5; 38.5)**				**Cell D5 (15.5; 37.5)**			
T	U	ϱ_U	C	ϱ_C	U	ϱ_U	C	ϱ_C	U	ϱ_U	C	ϱ_C	U	ϱ_U	C	ϱ_C	U	ϱ_U	C	ϱ_C
(s)	(km/s)	(km/s)	(km/s)	(km/s)	(km/s)	(km/s)	(km/s)	(km/s)	(km/s)	(km/s)	(km/s)	(km/s)	(km/s)	(km/s)	(km/s)	(km/s)	(km/s)	(km/s)	(km/s)	(km/s)
10	2.12	0.1			2.16	0.1			2.25	0.11			2.35	0.11			2.18	0.2		
15	2.32	0.08			2.29	0.08			2.33	0.09			2.41	0.1			2.45	0.16		
20	2.54	0.07			2.46	0.07			2.45	0.07			2.52	0.08			2.71	0.14		
25	2.8	0.07	3.67	0.22	2.76	0.07	3.66	0.22	2.79	0.08	3.66	0.22	2.86	0.09	3.65	0.22	2.99	0.15	3.7	0.22
30	3.03	0.08	3.71	0.18	3.04	0.08	3.7	0.18	3.11	0.08	3.7	0.18	3.2	0.09	3.69	0.18	3.16	0.16	3.72	0.18
35	3.25	0.16	3.76	0.16	3.28	0.16	3.76	0.16	3.36	0.16	3.75	0.16	3.46	0.16	3.75	0.16	3.31	0.32	3.77	0.16
50			3.85	0.12			3.85	0.12			3.85	0.12			3.85	0.12			3.85	0.12
80			3.92	0.12			3.92	0.12			3.92	0.12			3.92	0.12			3.92	0.12
100			3.98	0.12			3.98	0.12			3.98	0.12			3.98	0.12			3.98	0.12
r.m.s.		0.07		0.09		0.07		0.09		0.07		0.09		0.07		0.09		0.12		0.09

Tab. 1 (*segue*)

	Cell D6 (16.5; 37.5)				Cell D7 (17.5; 37.5)				Cell D8 (18.5; 37.5)			
T	U	ϱ_U	C	ϱ_C	U	ϱ_U	C	ϱ_C	U	ϱ_U	C	ϱ_C
(s)	(km/s)	(km/s)	(km/s)	(km/s)	(km/s)	(km/s)	(km/s)	(km/s)	(km/s)	(km/s)	(km/s)	(km/s)
10	2.18	0.1			2.2	0.1			2.24	0.1		
15	2.43	0.09			2.39	0.09			2.36	0.09		
20	2.67	0.08			2.61	0.09			2.56	0.09		
25	2.93	0.09	3.69	0.22	2.87	0.09	3.68	0.22	2.82	0.08	3.67	0.22
30	3.12	0.09	3.72	0.18	3.1	0.08	3.71	0.18	3.11	0.08	3.7	0.18
35	3.3	0.16	3.76	0.16	3.32	0.16	3.76	0.16	3.37	0.16	3.76	0.16
50			3.85	0.12			3.85	0.12			3.85	0.12
80			3.92	0.12			3.92	0.12			3.91	0.12
100			3.98	0.12			3.98	0.12			3.98	0.12
r.m.s.		0.07		0.09		0.07		0.09		0.07		0.09

The parameterization of the structure to be inverted is chosen taking into account the resolving power of the data [68, 90] and relevant petrological information [1, 12, 33, 55, 112]. Thus we fix the upper limit of V_s for the sub-Moho mantle at 4.9 km/s and the lower limit of V_s for the asthenosphere at depths greater than about 80 km at 4.0 km/s. The adopted parameterization with the variability range and the incremental steps for each parameter P_i (i = 1, …, 10) are reported in Tab. 2.

The available interpretations of the seismic profiles that cross most of the Italian peninsula and adjacent seas and other information available from literature (see the caption of Tab. 2 for the references) are used to fix h and V_p of the uppermost crustal layers, assuming that they are formed by Poissonian solids. The thickness of the water layer is chosen according to standard bathymetric maps. The density of all the layers is fixed in agreement with the Nafe-Drake relation, as reported by [50]. In most of the cells of the study area, one and the same relation between V_s, V_p and ϱ has been used for all the dependent parameters in the inversion. In cells A2, A3, B1, B2, B3 and B4 in Fig. 1, we have used the value of $V_p/V_s = 2.0$ (see Tab. 2), in agreement with the geophysical, geochemical and petrological model of the sub-marine lithosphere proposed by [12]. Inversion experiments performed considering values of V_p/V_s smaller than 2.0 supply sets of solutions that do not differ significantly from the ones discussed here. However, we prefer high V_p/V_s also because it gives the largest number of solutions in each cell, all the other elements of the parameterization remaining unchanged. According to the results of [90] this means that high V_p/V_s is more consistent with the data than a low one. The deeper structure, below the inverted layers, is the same for all the considered cells and it has been fixed according to already published data [41].

Let $V(T_i)$ and the standard deviation $\sigma(T_i)$ to be considered equal to $U(T_i)$ and

Tab. 2 - Parameterization used in the non-linear inversion. *Grey area*: h (thickness), V_s and V_p of each layer. The uppermost layers are fixed on the basis of available literature [22, 23, 24, 29, 31, 34, 35, 36, 40, 45, 46, 47, 48, 66, 77, 80, 85, 86, 108, 115]. The variable parameters are Pi, with i = 1, ... 5 for thickness and i = 6, ... 10 for V_s. *White area*: step (δPi) and the a priori allowed variability range for each parameter Pi.

Cell A2 (12.5; 40.5)			**Cell A3 (13.5; 40.5)**			**Cell A4 (14.5; 40.5)**			**Cell B1 (11.5; 39.5)**			**Cell B2 (12.5; 39.5)**			**Cell B3 (13.5; 39.5)**		
h	V_S	V_P	h	V_S	V_P	h	V_S	V_P	h	V_S	V_P	h	V_S	V_P	h	V_S	V_P
(km)	(km/s)	(km/s)	(km)	(km/s)	(km/s)	(km)	(km/s)	(km/s)	(km)	(km/s)	(km/s)	(km)	(km/s)	(km/s)	(km)	(km/s)	(km/s)
3	0.0	1.52	1.5	0.0	1.52	0.5	0.0	1.52	3	0.0	1.52	3	0.0	1.52	3.2	0.0	1.52
0.7	1.2	2.05	2.2	1.2	2.05	1	2.6	4.5	0.7	1.2	2.05	0.7	1.2	2.05	0.5	1.2	2.05
1	3.45	6.0	1	3.45	6.0	1.5	3.0	5.2	1	3.45	6.0	1	3.45	6.0	1	3.45	6.0
2	4.0	6.9	2	4.0	6.9	3	3.35	5.8	2	4.0	6.9	2	4.0	6.9	2	4.0	6.9
P1	P6	P6x1.73	P1	P6	P6x1.73	P1	P6	P6x1.73	P1	P6	P6x1.73	P1	P6	P6x1.73	P1	P6	P6x1.73
P2	P7	P7x2.00	P2	P7	P7x2.00	P2	P7	P7x1.73	P2	P7	P7x2.00	P2	P7	P7x2.00	P2	P7	P7x2.00
P3	P8	P8x2.00	P3	P8	P8x2.00	P3	P8	P8x1.73	P3	P8	P8x2.00	P3	P8	P8x2.00	P3	P8	P8x2.00
P4	P9	P9x2.00	P4	P9	P9x2.00	P4	P9	P9x1.73	P4	P9	P9x2.00	P4	P9	P9x2.00	P4	P9	P9x2.00
P5	P10	P10x2.00	P5	P10	P10x2.00	P5	P10	P10x1.73	P5	P10	P10x2.00	P5	P10	P10x2.00	P5	P10	P10x2.00
h	Step	Range	h	Step	Range	h	Step	Range	h	Step	Range	h	Step	Range	h	Step	Range
(km)	(km)	(km)	(km)	(km)	(km)	(km)	(km)	(km)	(km)	(km)	(km)	(km)	(km)	(km)	(km)	(km)	(km)
P1	4	2-14	P1	4	3-23	P1	4	5-25	P1	4.5	6.5-20	P1	4	2-18	P1	3	3.5-12.5
P2	10	10-30	P2	7.5	5.5-28	P2	8	6-22	P2	10	11-31	P2	7	8-29	P2	4	6-18
P3	40	10-50	P3	15	20-50	P3	12.5	10-47.5	P3	40	11-51	P3	20	20-60	P3	20	30-70
P4	50	55-105	P4	45	15-105	P4	55	50-105	P4	60	45-105	P4	50	45-95	P4	70	35-105
P5	70	70-140	P5	60	70-130	P5	70	60-130	P5	70	60-130	P5	80	55-135	P5	70	60-130
V_S	Step	Range	V_S	Step	Range	V_S	Step	Range	V_S	Step	Range	V_S	Step	Range	V_S	Step	Range
(km/s)	(km/s)	(km/s)	(km/s)	(km/s)	(km/s)	(km/s)	(km/s)	(km/s)	(km/s)	(km/s)	(km/s)	(km/s)	(km/s)	(km/s)	(km/s)	(km/s)	(km/s)
P6	0.3	3.4-4.6	P6	0.40	3.20-4.40	P6	0.2	2.55-4.15	P6	0.3	3.1-4.6	P6	0.2	3.1-4.5	P6	0.15	3.6-4.65
P7	0.4	2.8-4.4	P7	0.25	3.10-4.60	P7	0.25	3.25-4.75	P7	0.3	2.8-4.6	P7	0.25	2.8-4.55	P7	0.2	2.5-4.1
P8	0.4	3.35-4.55	P8	0.40	3.25-4.45	P8	0.5	3.35-4.85	P8	0.25	3.4-4.65	P8	0.4	3.3-4.5	P8	0.1	3.7-4.7
P9	0.15	4.0-4.75	P9	0.25	4.00-4.75	P9	0.25	4.0-4.75	P9	0.35	4.0-4.7	P9	0.3	4.0-4.9	P9	0.25	4.0-4.75
P10	0.3	4.0-4.9	P10	0.20	4.00-4.80	P10	0.25	4.0-4.75	P10	0.3	4.0-4.9	P10	0.3	4.0-4.9	P10	0.3	4.0-4.9

Tab. 2 (*segue*)

Cell B4 (14.5; 39.5)			Cell B5 (15.5; 39.5)			Cell B6 (16.5; 39.5)			Cell B7 (17.5; 39.5)			Cell C1 (11.5; 38.5)			Cell C2 (12.5; 38.5)		
h	V_S	V_P	h	V_S	V_P	h	V_S	V_P	h	V_S	V_P	h	V_S	V_P	h	V_S	V_P
(km)	(km/s)	(km/s)	(km)	(km/s)	(km/s)	(km)	(km/s)	(km/s)	(km)	(km/s)	(km/s)	(km)	(km/s)	(km/s)	(km)	(km/s)	(km/s)
2.5	0.0	1.52	0.9	0.0	1.52	4	2.45	4.25	1.5	0.0	1.52	1.5	0.0	1.52	1	0.0	1.52
0.5	1.3	2.24	2.1	1.15	1.98	9	2.8	4.85	1.5	2.9	5.0	0.9	1.1	1.9	1.4	1.1	1.9
2	3.45	6.0	3	2.9	5.0				2	3.52	6.1	0.4	2.31	4.0	0.4	2.31	4.0
1.5	4.0	6.9										4.2	2.90	5.0	3.2	2.9	5.0
P1	P6	P6x1.73	P1	P6	P6x1.73	P1	P6	P6x1.73	P1	P6	P6x1.73	P1	P6	P6x1.73	P1	P6	P6x1.73
P2	P7	P7x2.00	P2	P7	P7x1.73	P2	P7	P7x1.73	P2	P7	P7x1.73	P2	P7	P7x1.73	P2	P7	P7x1.73
P3	P8	P8x2.00	P3	P8	P8x1.73	P3	P8	P8x1.73	P3	P8	P8x1.73	P3	P8	P8x1.73	P3	P8	P8x1.73
P4	P9	P9x2.00	P4	P9	P9x1.73	P4	P9	P9x1.73	P4	P9	P9x1.73	P4	P9	P9x1.73	P4	P9	P9x1.73
P5	P10	P10x2.00	P5	P10	P10x1.73	P5	P10	P10x1.73	P5	P10	P10x1.73	P5	P10	P10x1.73	P5	P10	P10x1.73
h	Step	Range	h	Step	Range	h	Step	Range	h	Step	Range	h	Step	Range	h	Step	Range
(km)	(km)	(km)	(km)	(km)	(km)	(km)	(km)	(km)	(km)	(km)	(km)	(km)	(km)	(km)	(km)	(km)	(km)
P1	4	5-21	P1	2	5-29	P1	8	12-20	P1	3	6-21	P1	9	12-30	P1	10	14-34
P2	10	10-30	P2	10	5-25	P2	12	12-36	P2	4	12-28	P2	30	15-45	P2	30	20-50
P3	40	25-65	P3	20	20-60	P3	20	25-45	P3	15	7.5-37.5	P3	30	40-70	P3	25	25-75
P4	30	35-95	P4	20	15-95	P4	50	45-95	P4	60	70-130	P4	40	40-80	P4	40	45-85
P5	55	15-130	P5	45	35-125	P5	60	65-125	P5	70	40-110	P5	55	45-100	P5	40	50-90
V_S	Step	Range	V_S	Step	Range	V_S	Step	Range	V_S	Step	Range	V_S	Step	Range	V_S	Step	Range
(km/s)	(km/s)	(km/s)	(km/s)	(km/s)	(km/s)	(km/s)	(km/s)	(km/s)	(km/s)	(km/s)	(km/s)	(km/s)	(km/s)	(km/s)	(km/s)	(km/s)	(km/s)
P6	0.1	2.4-4.6	P6	0.05	2.5-4.6	P6	0.4	2.8-4.4	P6	0.2	2.45-4.25	P6	0.4	3.35-4.55	P6	0.3	3.15-4.65
P7	0.3	3.25-4.75	P7	0.2	3.2-4.6	P7	0.8	2.9-4.5	P7	0.4	2.7-4.3	P7	0.5	3.2-4.7	P7	0.25	3.25-4.5
P8	0.1	3.5-4.7	P8	0.1	3.45-4.85	P8	0.4	3.5-4.7	P8	0.5	3.2-4.7	P8	0.3	3.7-4.6	P8	0.6	3.4-4.6
P9	0.4	4.0-4.8	P9	0.1	4.0-4.8	P9	0.4	4.0-4.8	P9	0.3	4.0-4.9	P9	0.2	4.0-4.8	P9	0.2	4.0-4.8
P10	0.3	4.0-4.9	P10	0.1	4.0-4.8	P10	0.8	4.0-4.8	P10	0.4	4.0-4.8	P10	0.4	4.0-4.8	P10	0.4	4.0-4.8

Tab. 2 (*segue*)

Cell C3 (13.5; 38.5)			Cell C4 (14.5; 38.5)			Cell C5 (15.5; 38.5)			Cell C6 (16.5; 38.5)			Cell C7 (17.5; 38.5)			Cell C8 (18.5; 38.5)		
h	V_S	V_P	h	V_S	V_P	h	V_S	V_P	h	V_S	V_P	h	V_S	V_P	h	V_S	V_P
(km)	(km/s)	(km/s)	(km)	(km/s)	(km/s)	(km)	(km/s)	(km/s)	(km)	(km/s)	(km/s)	(km)	(km/s)	(km/s)	(km)	(km/s)	(km/s)
2	0.0	1.52	2.2	0.0	1.52	1	0.0	1.52	4	2.5	4.3	2.4	0.0	1.52	2.9	0.0	1.52
0.4	1.1	1.9	0.2	1.0	1.75	2	2.6	4.5	9	2.85	4.9	2.1	2.1	3.63	1.2	2.25	3.9
0.4	2.31	4.0	0.4	2.31	4.0							0.7	2.25	3.9	1.1	2.35	4.05
3.2	2.9	5.0	3.2	3.55	6.15							2.8	3.25	5.62	2.8	3.35	5.8
P1	P6	P6x1.73	P1	P6	P6x1.73	P1	P6	P6x1.73	P1	P6	P6x1.73	P1	P6	P6x1.73	P1	P6	P6x1.73
P2	P7	P7x1.73	P2	P7	P7x1.73	P2	P7	P7x1.73	P2	P7	P7x1.73	P2	P7	P7x1.73	P2	P7	P7x1.73
P3	P8	P8x1.73	P3	P8	P8x1.73	P3	P8	P8x1.73	P3	P8	P8x1.73	P3	P8	P8x1.73	P3	P8	P8x1.73
P4	P9	P9x1.73	P4	P9	P9x1.73	P4	P9	P9x1.73	P4	P9	P9x1.73	P4	P9	P9x1.73	P4	P9	P9x1.73
P5	P10	P10x1.73	P5	P10	P10x1.73	P5	P10	P10x1.73	P5	P10	P10x1.73	P5	P10	P10x1.73	P5	P10	P10x1.73
h	Step	Range	h	Step	Range	h	Step	Range	h	Step	Range	h	Step	Range	h	Step	Range
(km)	(km)	(km)	(km)	(km)	(km)	(km)	(km)	(km)	(km)	(km)	(km)	(km)	(km)	(km)	(km)	(km)	(km)
P1	2	7-25	P1	2	5-19	P1	4	2-22	P1	4	4-16	P1	5	15-30	P1	5	10-30
P2	5	5-30	P2	4	10-34	P2	4	4-28	P2	15	2.5-32.5	P2	15	25-40	P2	15	15-30
P3	20	20-80	P3	5	20-50	P3	10	5-35	P3	10	10-30	P3	20	35-55	P3	25	25-50
P4	30	25-85	P4	15	25-100	P4	50	60-110	P4	60	65-125	P4	50	50-100	P4	50	50-100
P5	60	55-115	P5	35	20-125	P5	60	70-130	P5	70	60-130	P5	60	45-105	P5	60	65-125
V_S	Step	Range	V_S	Step	Range	V_S	Step	Range	V_S	Step	Range	V_S	Step	Range	V_S	Step	Range
(km/s)	(km/s)	(km/s)	(km/s)	(km/s)	(km/s)	(km/s)	(km/s)	(km/s)	(km/s)	(km/s)	(km/s)	(km/s)	(km/s)	(km/s)	(km/s)	(km/s)	(km/s)
P6	0.1	2.55-4.35	P6	0.05	2.45-4.55	P6	0.15	2.3-4.25	P6	0.3	2.7-4.5	P6	0.1	2.4-4.2	P6	0.05	2.45-4.55
P7	0.05	3.05-4.55	P7	0.20	3.05-4.55	P7	0.4	3.15-4.75	P7	0.5	3.4-4.4	P7	0.3	3.35-4.55	P7	0.4	3.1-4.7
P8	0.1	3.6-4.8	P8	0.10	3.30-4.70	P8	0.2	3.1-4.7	P8	0.5	3.1-4.6	P8	0.4	3.9-4.7	P8	0.3	3.35-4.85
P9	0.2	4.0-4.8	P9	0.05	4.00-4.80	P9	0.2	4.0-4.8	P9	0.2	4.0-4.8	P9	0.8	4.0-4.8	P9	0.75	4.0-4.75
P10	0.4	4.0-4.8	P10	0.10	4.00-4.80	P10	0.25	4.0-4.75	P10	0.25	4.0-4.75	P10	0.8	4.0-4.8	P10	0.8	4.0-4.8

Tab. 2 (*segue*)

Cell C9 (19.5; 38.5)			Cell D5 (15.5; 37.5)			Cell D6 (16.5; 37.5)			Cell D7 (17.5; 37.5)			Cell D8 (18.5; 37.5)		
h	V_S	V_P	h	V_S	V_P	h	V_S	V_P	h	V_S	V_P	h	V_S	V_P
(km)	(km/s)	(km/s)	(km)	(km/s)	(km/s)	(km)	(km/s)	(km/s)	(km)	(km/s)	(km/s)	(km)	(km/s)	(km/s)
3	0.0	1.52	2.5	0.0	1.52	2.7	0.0	1.52	3	0.0	1.52	2.9	0.0	1.52
1	2.02	3.5	1.6	2.25	3.9	1.4	2.25	3.9	1.1	2.25	3.90	1.2	2.25	3.9
			1.1	2.35	4.05	1.1	2.35	4.05	1.1	2.35	4.05	1.1	2.35	4.05
			2.8	3.35	5.8	2.8	3.35	5.8	2.8	3.35	5.80	2.8	3.35	5.8
P1	P6	P6x1.73	P1	P6	P6x1.73	P1	P6	P6x1.73	P1	P6	P6x1.73	P1	P6	P6x1.73
P2	P7	P7x1.73	P2	P7	P7x1.73	P2	P7	P7x1.73	P2	P7	P7x1.73	P2	P7	P7x1.73
P3	P8	P8x1.73	P3	P8	P8x1.73	P3	P8	P8x1.73	P3	P8	P8x1.73	P3	P8	P8x1.73
P4	P9	P9x1.73	P4	P9	P9x1.73	P4	P9	P9x1.73	P4	P9	P9x1.73	P4	P9	P9x1.73
P5	P10	P10x1.73	P5	P10	P10x1.73	P5	P10	P10x1.73	P5	P10	P10x1.73	P5	P10	P10x1.73
h	Step	Range	h	Step	Range	h	Step	Range	h	Step	Range	h	Step	Range
(km)	(km)	(km)	(km)	(km)	(km)	(km)	(km)	(km)	(km)	(km)	(km)	(km)	(km)	(km)
P1	3	4-13	P1	10	15-25	P1	7.5	10-25	P1	3	7-25	P1	2.5	5-30
P2	8	8-24	P2	15	20-35	P2	20	10-30	P2	15	10-25	P2	15	20-35
P3	20	10-50	P3	25	20-45	P3	20	20-40	P3	40	20-60	P3	20	20-40
P4	60	70-130	P4	40	70-110	P4	45	20-110	P4	40	50-90	P4	50	55-105
P5	60	60-120	P5	60	65-125	P5	60	65-125	P5	60	65-125	P5	60	65-125
V_S	Step	Range	V_S	Step	Range	V_S	Step	Range	V_S	Step	Range	V_S	Step	Range
(km/s)	(km/s)	(km/s)	(km/s)	(km/s)	(km/s)	(km/s)	(km/s)	(km/s)	(km/s)	(km/s)	(km/s)	(km/s)	(km/s)	(km/s)
P6	0.8	2.75-4.35	P6	0.25	3.0-4.5	P6	0.1	2.45-4.25	P6	0.1	2.8-4.35	P6	0.1	2.8-4.6
P7	0.3	2.5-4.3	P7	0.4	3.3-4.5	P7	0.3	3.4-4.6	P7	0.4	3.8-4.6	P7	0.4	3.55-4.75
P8	0.4	3.05-4.65	P8	0.35	3.45-4.85	P8	0.4	3.55-4.75	P8	0.3	4.0-4.6	P8	0.4	3.45-4.65
P9	0.3	4.0-4.9	P9	0.4	4.0-4.8	P9	0.4	4.0-4.8	P9	0.6	4.0-4.6	P9	0.6	4.0-4.6
P10	0.4	4.0-4.8	P10	0.8	4.0-4.8	P10	0.8	4.0-4.8	P10	0.8	4.0-4.8	P10	0.7	4.0-4.7

$\sigma_U(T_i)$ for the group velocity case, or equal to $C(T_i)$ and $\sigma_C(T_i)$ for the phase velocity case and the parameter P_j to vary by an amount δP_j from its starting value: since the parameterization has been made generally following the condition that the parameter steps, δP_j, are minima, subject to the condition $\sum_j \left(\frac{\partial V(T_i)}{\partial P_j} \right) \delta P_j = \sigma(T_i)$ [68, 90], the parameter steps δP_j used in the non-linear inversion represent an acceptable approximation for the uncertainty of the P_i estimates (see Tab. 2).

RESOLVING POWER

The depth resolution of our dataset is determined by the partial derivatives [122] of the dispersion curves of the Rayleigh wave fundamental mode with respect

to the shear-wave velocity at different periods. The vertical resolution of the considered dispersion measurements is consistent with the steps given in Tab. 2 and extends to depth of the order of 250 km [25].

The lateral resolution of the dispersion measurements (phase and group velocities) performed by [111] is about 2°x2°. In fact, the grouping of group velocity dispersion relations has allowed identifying areas with similar dispersion properties, but not necessarily with laterally homogeneous structures. The resolution of dispersion measurements is, in fact, only indirectly connected with the lateral structural resolution: to a given dispersion relation can correspond different structural models, depending upon the a priori information to be used to constrain the inversion. In the following we present a numerical test, in analogy with the situation depicted by cells C5, C6 and C7, showing that dispersion curves that differ for $T \leq 25$ s but are identical at longer periods (Fig. 3 and Tab. 3), can be consistent with significantly different models, depending upon the constraints imposed by the a priori knowledge.

The non-linear inversion is performed for each analyzed case considering different crustal models, e.g. oceanic-like and continental-like: in cases 1 and 3 the uppermost part of the crustal model contains a water layer (1 km and 2.4 km thick, respec-

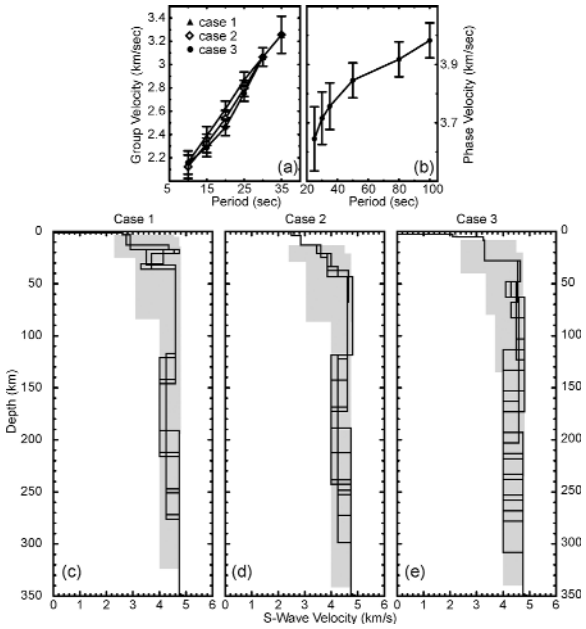

Fig. 3 - (a) Group velocity curves of three tested cases: the velocity is the same at the period of 30 and 35 s.; (b) Phase velocity curve common to the three cases; (c, d, e) Sets of solutions (thin lines) obtained through the non–linear inversion of the dispersion relations of each case. The investigated parameter's space (grey zone) is shown as well.

Tab. 3 - Group (U) and phase (C) velocity values at different periods (from 10 s to 35 s and from 25 s to 100 s, respectively) with the single point error (ϱ_U, ϱ_C) and the r.m.s. values for the three cases of the test. Phase velocities at all the periods and group velocities at the periods of 30 and 35 s have the same values for the three cases and the slightly different group velocity values, in the period range 10-25 s, are shaded.

	Case 1				Case 2				Case 3			
T	U	ϱ_U	C	ϱ_C	U	ϱ_U	C	ϱ_C	U	ϱ_U	C	ϱ_C
(s)	(km/s)	(km/s)	(km/s)	(km/s)	(km/s)	(km/s)	(km/s)	(km/s)	(km/s)	(km/s)	(km/s)	(km/s)
10	2.16	0.1			2.12	0.1			2.16	0.1		
15	2.39	0.08			2.32	0.08			2.29	0.08		
20	2.62	0.07			2.54	0.07			2.46	0.07		
25	2.87	0.07	3.65	0.11	2.8	0.07	3.65	0.11	2.76	0.07	3.65	0.11
30	3.07	0.08	3.72	0.09	3.07	0.08	3.72	0.09	3.07	0.08	3.72	0.09
35	3.26	0.16	3.76	0.08	3.26	0.16	3.76	0.08	3.26	0.16	3.76	0.08
50			3.85	0.08			3.85	0.06			3.85	0.06
80			3.92	0.06			3.92	0.06			3.92	0.06
100			3.98	0.06			3.98	0.06			3.98	0.06
r.m.s.		0.07		0.55		0.07		0.55		0.07		0.55

tively), that is absent in case 2. The sets of solutions obtained for each case, using the parameterization presented in Tab. 4, are shown in Fig. 3. Even if the a priori constraint is limited to the uppermost crust, a clear cut differentiation in the lower crust and upper mantle structural properties extends to about 50 km, and the retrieved differences tend to fade out only at depths greater than 100 km. Thus, even if different cells are characterised by equal phase velocities, but by slightly different group velocities and by different a priori constraint at crustal level, the set of solutions of the inverse problem can be quite different even at mantle depths. In other words, the introduction of independent a priori information about the crustal parameters improves the resolving power of our tomography data at greater depths [25].

Average models

The set of solutions (V_s versus depth) for all the cells, from the surface to the depth of 250 km, are shown in Fig. 4. In each frame, the solutions (thin lines), the explored part of the parameters space (grey area), the chosen solution (bold line) for each cell are shown; M stands for Mohorovicic discontinuity, or Moho. At the base of our choice of the solution for each cell there is a tenet of modern science known as Occam's razor: it is vain to do with more what can be done with fewer [114]. In other words a simple solution is preferable to one that is unnecessarily complicated [32].

Tab. 4 - Parameterization used in the non-linear inversion of the test. *Grey area*: h (thickness), V_s and V_p of each layer. The uppermost layers are fixed differently from the three cases. The variable parameters are Pi, with i = 1, … 5 for thickness and i = 6, … 10 for V_s. *White area*: step (δPi) and the variability range for each parameter Pi.

Case 1			Case 2			Case 3		
h	V_S	V_P	h	V_S	V_P	h	V_S	V_P
(km)	(km/s)	(km/s)	(km)	(km/s)	(km/s)	(km)	(km/s)	(km/s)
1	0.0	1.52	4	2.5	4.3	2.4	0.0	1.52
2	2.6	4.5	9	2.85	4.9	2.1	2.1	3.63
						0.7	2.25	3.9
						2.8	3.25	5.62
P1	P6	P6x1.73	P1	P6	P6x1.73	P1	P6	P6x1.73
P2	P7	P7x1.73	P2	P7	P7x1.73	P2	P7	P7x1.73
P3	P8	P8x1.73	P3	P8	P8x1.73	P3	P8	P8x1.73
P4	P9	P9x1.73	P4	P9	P9x1.73	P4	P9	P9x1.73
P5	P10	P10x1.73	P5	P10	P10x1.73	P5	P10	P10x1.73
h	Step	Range	h	Step	Range	h	Step	Range
(km)	(km)	(km)	(km)	(km)	(km)	(km)	(km)	(km)
P1	4	2-22	P1	4	8-16	P1	4	12-32
P2	10	4-24	P2	5	12.5-27.5	P2	20	20-40
P3	10	5-35	P3	20	10-30	P3	20	15-55
P4	25	60-110	P4	50	25-125	P4	50	50-100
P5	60	70-130	P5	60	70-130	P5	25	55-105
V_S	Step	Range	V_S	Step	Range	V_S	Step	Range
(km/s)	(km/s)	(km/s)	(km/s)	(km/s)	(km/s)	(km/s)	(km/s)	(km/s)
P6	0.15	2.3-4.55	P6	0.15	2.4-4.5	P6	0.1	2.4-4.5
P7	0.2	3.15-4.75	P7	0.15	3.25-4.75	P7	0.1	3.35-4.75
P8	0.2	3.1-4.7	P8	0.4	3.05-4.65	P8	0.2	3.7-4.7
P9	0.2	4.0-4.8	P9	0.2	4.0-4.8	P9	0.2	4.0-4.8
P10	0.25	4.0-4.75	P10	0.25	4.0-4.75	P10	0.25	4.0-4.75

Therefore, our choice starts in cells B5 and C5, where the distribution of the intermediate and deep earthquakes is correlated with the largest seismic velocities, and moves to the neighbouring cells preserving only robust lateral variations. We consider the ISC catalogue [61] and, to have a gross estimate of the seismic energy released, E, we use the relation Log E = 11.8+1.5M_s proposed by [57]. Where necessary, we transform m_b into M_s using the relations of [107], correcting M_s for focal depth as indicated by [60]. The distribution of the energy versus depth is calculated in each cell grouping the events in 15 km depth intervals.

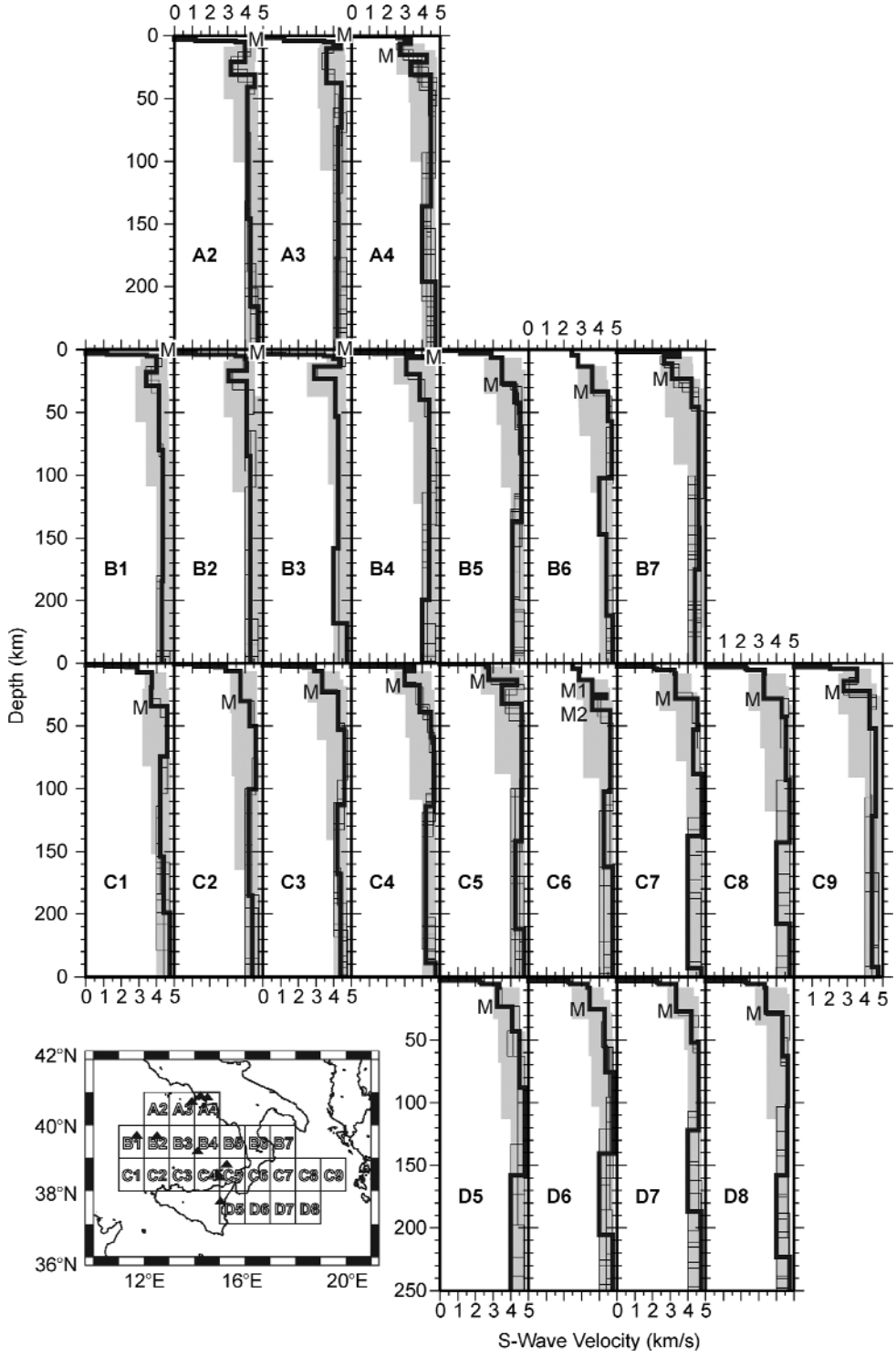

Fig. 4 - Set of solutions (thin lines) obtained through the non–linear inversion of the dispersion relations of each cell. The investigated parameter's space (grey zone) and the chosen solution (bold line) are shown as well. The Moho is marked with M. M1 and M2, in cell C6, mark the lithospheric doubling.

To reduce the effects of the projection of possible systematic errors into the inverted model, the r.m.s. of the chosen solution does not correspond to the minimum r.m.s., but it is as close as possible to the average value of r.m.s., which is computed from all the solutions. If alternatively a median solution of all the solutions in a set is used as representative [116], although it may not represent a formally acceptable solution of the inversion process, the resulting picture is not significantly different from the one shown in Fig. 4. The chosen structural models satisfy (within the r.m.s. value used in our inversion; see Tab. 1) the additional condition to be consistent, at periods greater than 35 s, with the group velocity values given by [102]. On the base of mathematical statistics, the point estimation of the parameters corresponding to the chosen solutions have little sense without the associated confidence interval, i.e. the values of V_s and thickness of the chosen solutions cannot be taken at face value. The assessment of the uncertainty affecting each inverted layer can be made through the parameterization steps [68, 90] and it is reported in Tab. 5 for the chosen models of all the study cells. In the following description we refer to the velocity and thickness values corresponding to the chosen solution taking into account the uncertainties and that the boundaries between layers can be transition zones in their own right.

1. *The Crust*

In cells A2-A3 and B1-B4 (see Fig. 4) the sedimentary layer is very thin and followed by a layering consistent with standard schematic oceanic crustal models [91]. All the other cells are characterised by a thicker crust, in which, in general, the velocity of the sediments increases with increasing depth. A low velocity layer appears in the crust, just above the Moho in A4, C4, C9 and D5 with V_s in the range 2.65-3.35 km/s, and in the upper crust in B7 (V_s in the range 2.55-2.75 km/s). Most of the cells in the continental region of Calabria and in the Tyrrhenian offshore of Sicily-Calabria (e.g. B5, B6, C1-C3 and C6) are characterised by layers, just above the Moho, with V_s in the range 3.3-3.95 km/s. The V_s just above the Moho in the Ionian cells B7, C7-C9 and D5-D8, instead, falls in the lower range 2.65-3.5 km/s. The Moho depth in each cell is defined within a few kilometres.

2. *The Moho and the uppermost Upper Mantle*

In the following, the term «mantle wedge» will be used to indicate the low velocity zone (V_s less than about 4.2 km/s) in the uppermost mantle overlying the high velocity lid (V_s greater than about 4.4 km/s). Thus, in the mantle wedge the percentage of partial melting is greater than 1%, according to [12].

In the north-western part of the study area (cells A2, A3 and B1-B3), the average Moho is very shallow (about 7 km deep) and the average lid thickness is about 10 km. Below this thin and strongly laterally variable lid (V_s in the range 3.85-4.4

Tab. 5 - Range of variability of the parameters h (thickness) and V_s for each layer of the chosen solutions. The inverted quantities are rounded off to 0.5 km or to 0.05km/s. The a priori information used to constrain the inversion is taken into account. Therefore, the chosen solution does not necessarily fall in the centre of the range that can be smaller than the step used in the inversion. The thickness marked by # is not a truly inverted parameter, but it satisfies the condition that the total thickness from the free surface to the top of the fixed upper mantle is equal to a predefined quantity H. In this study H = 349 km. The structure deeper that H is the same for all the considered cells and it has been fixed according to already published models [41].

Cell A2 (12.5;40.5)		**Cell A3 (13.5;40.5)**		**Cell A4 (14.5;40.5)**		**Cell B1 (11.5;39.5)**		**Cell B2 (12.5;39.5)**		**Cell B3 (13.5;39.5)**		**Cell B4 (14.5;39.5)**		**Cell B5 (15.5;39.5)**		**Cell B6 (16.5;39.5)**	
h	V_S	h	V_S	h	V_S	h	V_S	h	V_S	h	V_S	h	V_S	h	V_S	h	V_S
(km)	(km/s)	(km)	(km/s)	(km)	(km/s)	(km)	(km/s)	(km)	(km/s)	(km)	(km/s)	(km)	(km/s)	(km)	(km/s)	(km)	(km/s)
3	0.0	1.5	0.0	0.5	0.0	3	0.0	3	0.0	3.2	0.0	2.5	0.0	0.9	0.0	4	2.45
0.7	1.2	2.2	1.2	1	2.6	0.7	1.2	0.7	1.2	0.5	1.2	0.5	1.3	2.1	1.15	9	2.8
1	3.45	1	3.45	1.5	3.0	1	3.45	1	3.45	1	3.45	2	3.45	3	2.9		
2	4.0	2	4.0	3	3.35	2	4.0	2	4.0	2	4.0	1.5	4.0				
12-14	3.85-4.15	3-5	4.2-4.4	7-11	2.65-2.85	8.5-13	3.85-4.15	8-12	4.0-4.2	5-8	4.25-4.4	11-15	3.05-3.15	20-22	3.45-3.5	6-24	3.4-3.8
10-15	3.0-3.4	24-28	3.55-3.75	6-10	4.1-4.35	11-16	3.25-3.55	8-11.5	2.9-3.15	8-12	2.8-3.0	15-25	3.7-4.0	10-20	4.1-4.3	18-24	4.1-4.5
10-30	4.35-4.55	27.5-42.5	4.25-4.45	10-16.25	3.1-3.6	31-51	4.0-4.25	50-60	3.9-4.3	30-40	4.05-4.15	45-65	4.35-4.45	30-50	4.5-4.6	35-55	4.5-4.7
80-105	4.05-4.2	82.5-105	4.1-4.35	77.5-105	4.35-4.6	75-105	4.15-4.5	45-70	4.15-4.45	70-105	4.1-4.35	80-95	4.2-4.6	45-65	4.55-4.65	45-70	4.0-4.2
80-105	4.15-4.45	70-100	4.1-4.3	60-95	4.0-4.15	95-130	4.15-4.45	95-135	4.15-4.45	60-95	4.0-4.15	102.5-130	4.0-4.15	102.5-125	4.05-4.15	65-95	4.0-4.8
#	4.75	#	4.75	#	4.75	#	4.75	#	4.75	#	4.75	#	4.75	#	4.75	#	4.75
44	4.9	44	4.9	44	4.9	44	4.9	44	4.9	44	4.9	44	4.9	44	4.9	44	4.9
Cell B7 (17.5;39.5)		**Cell C1 (11.5;38.5)**		**Cell C2 (12.5;38.5)**		**Cell C3 (13.5;38.5)**		**Cell C4 (14.5;38.5)**		**Cell C5 (15.5;38.5)**		**Cell C6 (16.5;38.5)**		**Cell C7 (17.5;38.5)**		**Cell C8 (18.5;38.5)**	
h	V_S	h	V_S	h	V_S	h	V_S	h	V_S	h	V_S	h	V_S	h	V_S	h	V_S
(km)	(km/s)	(km)	(km/s)	(km)	(km/s)	(km)	(km/s)	(km)	(km/s)	(km)	(km/s)	(km)	(km/s)	(km)	(km/s)	(km)	(km/s)
1.5	0.0	1.5	0.0	1	0.0	2	0.0	2.2	0.0	1	0.0	4	2.5	2.4	0.0	2.9	0.0
1.5	2.9	0.9	1.1	1.4	1.1	0.4	1.1	0.2	1.0	2	2.6	9	2.85	2.1	2.1	1.2	2.25
2	3.52	0.4	2.31	0.4	2.31	0.4	2.31	0.4	2.31					0.7	2.25	1.1	2.35
		4.2	2.9	3.2	2.9	3.2	2.9	3.2	3.55					2.8	3.25	2.8	3.35
6-7.5	2.55-2.75	12-16.5	3.55-3.95	19-29	3.6-3.9	16-18	3.3-3.4	10-12	2.95-3.0	8-12	2.65-2.8	10-14	3.45-3.75	17.5-22.5	3.25-3.35	17.5-22.5	3.25-3.3
12-14	2.9-3.3	15-30	3.45-3.95	20-35	4.1-4.35	27.5-30	4.2-4.25	20-24	3.75-3.95	4-6	4.15-4.55	2.5-10	4.15-4.4	25-32.5	4.4-4.55	15-22.5	4.1-4.5
15-30	3.95-4.45	40-55	4.45-4.6	37.5-62.5	4.3-4.6	50-70	4.55-4.65	17.5-22.5	4.45-4.55	10-20	3.4-3.6	10-15	3.35-3.85	35-45	4.1-4.5	37.5-50	4.4-4.7
100-130	4.45-4.75	60-80	4.1-4.3	65-85	4.1-4.3	40-70	4.1-4.3	47.5-62.5	4.6-4.65	85-110	4.5-4.7	65-95	4.5-4.7	50-75	4.4-4.8	50-75	4.35-4.75
75-110	4.2-4.6	45-72.5	4.2-4.6	70-90	4.2-4.6	85-115	4.2-4.6	107.5-125	4.15-4.25	70-100	4.1-4.35	60-95	4.1-4.35	75-105	4.0-4.4	65-95	4.0-4.4
#	4.75	#	4.75	#	4.75	#	4.75	#	4.75	#	4.75	#	4.75	#	4.75	#	4.75
44	4.9	44	4.9	44	4.9	44	4.9	44	4.9	44	4.9	44	4.9	44	4.9	44	4.9

Tab. 5 (*segue*)

Cell C9 (19.5;38.5)		Cell D5 (15.5;37.5)		Cell D6 (16.5;37.5)		Cell D7 (17.5;37.5)		Cell D8 (18.5;37.5)	
h	V_S	h	V_S	h	V_S	h	V_S	h	V_S
(km)	(km/s)	(km)	(km/s)	(km)	(km/s)	(km)	(km/s)	(km)	(km/s)
3	0.0	2.5	0.0	2.7	0.0	3	0.0	2.9	0.0
1	2.02	1.6	2.25	1.4	2.25	1.1	2.25	1.2	2.25
		1.1	2.35	1.1	2.35	1.1	2.35	1.1	2.35
		2.8	3.35	2.8	3.35	2.8	3.35	2.8	3.35
8.5-11.5	3.15-3.95	15-20	3.1-3.35	13.5-21	3.4-3.5	17.5-20.5	3.3-3.4	18.5-21	3.35-3.45
8-12	2.65-2.95	20-27.5	3.9-4.3	20-30	4.15-4.45	17.5-25	4.0-4.4	27.5-35	4.15-4.55
20-40	4.05-4.45	32.5-45	4.3-4.65	20-30	4.15-4.55	20-40	4.45-4.6	30-40	4.45-4.65
70-100	4.45-4.75	70-90	4.6-4.8	42.5-87.5	4.6-4.8	50-70	4.3-4.6	55-80	4.3-4.6
90-120	4.2-4.6	95-125	4.0-4.4	65-95	4.0-4.4	65-95	4.0-4.4	65-95	4.0-4.35
#	4.75	#	4.75	#	4.75	#	4.75	#	4.75
44	4.9	44	4.9	44	4.9	44	4.9	44	4.9

km/s, with the maximum in cell B3), there is a very well developed low velocity layer (V_s in the range 2.8-3.75 km/s) with variable thickness (in the range 8-28 km) and centred at a depth of about 22 km. A similar layering is found in the uppermost 30 km of cell A4, the main difference being a deeper Moho, at a depth of about 15 km. In B4 the low velocity zone is characterised by two layers, with V_s increasing from 3.05-3.15 km/s, just below a very thin lid, to 3.7-4.0 km/s. Following our definition of mantle wedge, we can state that it is present in cells A2-A4 and has its bottom at a depth of about 30-40 km, whilst, since in cells B1-B4 the V_s just below the very low velocity layer is lower than 4.4 km/s (in the range 3.9-4.45 km/s), we identify the low velocity zone like an uppermost asthenosphere (see below for more explanations). In this north-western Tyrrhenian area the V_s in the uppermost upper mantle is consistent with a high percentage of partial melting (about 10% according to [12]). This regional feature, in cells B1-B4, is well compatible with the presence of anomalous shallow mantle materials reported by [120] in correspondence of the huge volcanic structures like the Vavilov-Magnaghi and the Marsili Seamounts; the shallow partial melting in cells A3 and A4 can be associated to Ischia, Phlegraean Fields and Vesuvius active volcanoes. In cells A2-A4, the mantle wedge (with V_s in the range 3.0-3.75 km/s), that surmounts the high velocity lid, is been originally detected by [18] and [93] and confirmed by the geochemical analysis by [73].

Going towards east (cells B5-B7) the Moho ranges at the depth of 19-37 km. The lid velocity increases with increasing depth, from about 4.0 to 4.75 km/s and the lid reaches the depth between 110 km and 190 km in B5 and B7 and less than 115 km in B6.

The structural models of cells C1-C5 are markedly different from those of cells B1-B4. In fact, the Moho depth varies from about 11 km to 53 km and the smallest value is reached in correspondence of the active Aeolian volcanic islands (cells C4 and C5). In cells C2-C3 there is a V_s gradient in the lid, which is about 60-100 km thick, whilst in cell C1 the relatively soft uppermost lid, characterising the sub-Moho material in cells C2 and C3, is not present. In C4, the V_s immediately below the Moho can be as low as 3.75 km/s (mantle wedge with about 3-4% of partial melting, according to [12]), while the high velocity lid is found at a depth larger than about 40 km. In C5 the relatively soft lid extends only to 15-21 km depth and it is on top of a low velocity (V_s in the range 3.4-3.6 km/s) layer, here designated as mantle wedge (about 10% of partial melting, according to [12]), which overlies a lithospheric root (V_s in the range 4.5-4.7 km/s) that reaches the maximum depth of about 150 km. This feature is visible in the vertical cross-section by [81] as well. The large amount of partial melting in C4 and C5 correlates well with the presence of the Aeolian volcanic islands (Lipari and Vulcano in C4 and Stromboli in C5).

The structural properties change abruptly in cell C6. Below a crust 23-27 km thick, and a very thin lid, there is a low velocity (V_s in the range 3.35-3.85 km/s) layer 10-15 km thick, on top of a layer with V_s in the range 4.5-4.7 km/s that reaches at least the depth of about 100 km. These properties, not imposed a priori in the inversion scheme and common to all models inverted for cell C6, can be interpreted as a lithospheric doubling and the deeper Moho can be seen at the depth of 36 km. A similar feature (lithospheric doubling) could be seen in cells B5 and B6, but it is not common to all possible solutions obtained in these cells.

Going towards east, in the Ionian zone of the study area (cells C7-C9, D5-D8), the Moho depth varies in the range between about 20 km and 30 km. In cell D5 a mantle wedge (V_s in the range 3.9-4.3 km/s) is detected just below the Moho and it overlies a high velocity lid (characterised by a positive gradient with increasing depth and the maximum V_s at about 4.8 km/s) that can reach the depth of 190 km. The average V_s of 4.1 km/s in the mantle wedge implies that the partial melting is around 1-2% [12]. In cells C8-C9 and D6-D8 the velocity in the lid, in general, increases with increasing depth, starting from a relatively low velocity layer at about 4.0-4.55 km/s just below the Moho and with the lithospheric thickness at least of 90 km. In cell C7, on the top of the layers characterising the lid of the previous cells, there is a relatively high velocity layer (in the range of 4.4-4.55 km/s) with variable thickness in the range 25-32.5 km. The lid terminates at a depth in the range from 135 to 185 km.

Starting from C8 and going towards the west (cell C5), the soft lid, with V_s about 4.1-4.5 km/s in C8-C7 and 4.1-4.35 km/s in C6-C5, deepens and its thickness increases from 15-22 km to 70-100 km. This soft lid layer overlies a high velocity layer that reaches a depth not less than 250 km in C5-C6. The structural setting depicted by the models for cells C5-C8 can be consistent with the subduction of a rifted continental Ionian lithosphere [72], formed during the Jurassic extensional phase.

3. *The Asthenosphere*

The properties below the uppermost upper mantle change significantly going from the Tyrrhenian Sea to the Sicily-Calabria offshore and to the Ionian Sea. In fact, the topography of the asthenosphere is very variable and its bottom can be shallower than about 170 km.

In cells A2-A3 the asthenosphere has V_s in the range 4.05-4.45 km/s and starts at the depth of 40-80 km. In the central part of the Tyrrhenian Sea study area (cells B1-B4) the asthenosphere is as shallow as about 10 km, and in cells B1-B3 it is characterised by a layering. In general V_s increases with increasing depth starting from 2.80-3.55 km/s to reach 4.05-4.45 km/s in the lower asthenosphere, which extends deeper than about 180 km. The structure of cell B4 does not satisfy our definition of mantle wedge, even if a relatively high velocity body is seen below the upper mantle low velocity layer. In fact the asthenosphere is perturbed by a layer with relatively high V_s (4.2-4.6 km/s), centred at a depth of about 110 km, that surmounts a well developed low velocity asthenosphere (V_s in the range 4.0-4.15 km/s), thicker than 100 km. This low velocity asthenospheric layer is present also in cell B5 centred at 160-225 km of depth.

The asthenospheric V_s in cells B6-B7 and C9 is poorly resolved by our data however the average value around 4.4 km/s is consistent with the measurements of [102]; the top of the asthenospheric layer is at a depth larger than 80 km, and the bottom reaches a depth larger than 250 km as in standard stable continental structures [89].

The asthenosphere of C1-C3 is characterised by a gradient with V_s between 4.1 km/s and 4.6 km/s, while the V_s is in the range 4.15-4.25 km/s in cell C4. In this area the asthenospheric layer starts at a depth larger than about 80 km and extends to a depth larger than 250 km.

In cells A4 and C5-C6 the relatively low velocity layer, in the range 4.0-4.35 km/s and with a thickness in the range 60-100 km, is below a high velocity layer, with V_s in the range 4.35-4.7 km/s, which has been also detected by [81]. This relatively low velocity layer could be interpreted as «possible» asthenosphere, but in the discussion, we give an alternative interpretation consistent with the subduction of the Ionian-Adria lithosphere.

In cells C7-C8 and D5-D8 the asthenospheric low velocity layer, with V_s in the range 4.0-4.4 km/s, starts at a depth larger than about 100 km and reaches a depth exceeding 250 km. In D5 a high velocity body (V_s in the range 4.3-4.8 km/s) separates the asthenosphere from the shallow mantle wedge with V_s in the range 3.9-4.3 km/s.

Discussion

A fine structure of the lithospheric mantle, i.e. its layering, is a common feature to the models of most of the cells. Our findings have been made possible thanks to the improved resolving power of the data of [111] with respect to the

one of the data used to depict the main features of the 3D shear-wave velocity structure beneath the European area by [41], [79], [81], [82] and [83].

The following interpretation of the obtained spatial distribution of V_s is performed comparing the structure of each cell in the study area with pertinent independent models [12, 40, 58, 65, 87, 89, 136].

1. *The Tyrrhenian Basin: Magnaghi-Vavilov and Marsili Seamounts*

The generalized presence of low seismic velocity in the Tyrrhenian Basin could be consistent with the mantle plume hypothesis formulated by [136]: our results are very similar to the upper mantle V_s model of the mid-ocean ridge, associated with shallow and passive upwelling, that is characterised by regions of low seismic velocity at depths shallower than 50 km (East Pacific Rise, Pacific-Antartic Ridge, Southeast Indian Ridge). Analogue models with low velocities in the upper mantle are found in Afar and western Saudi Arabia by [59], [69], [76]. The East African Rift model, proposed by [69], shows an extensive low velocity zone in the upper mantle with a V_s retardation of about 4% attributed to elevated temperature and partial melting. The presence of a very low V_s below a thin lid (Fig. 4) makes the central part of the Southern Tyrrhenian Sea (cells B1-B4) some how similar to the models formulated by [12] for the oceanic lithosphere within few tens of kilometres from the ridge axis. The identification of oceanic ridge structural properties is in agreement with the compilations by [87] and [89] about the average crust and uppermost mantle velocity models that represent the various phases of the evolutionary process from the break-up of a continent to the generation of new oceanic crust/lithosphere in the ridge. In the central Tyrrhenian area (cells A2-A3, B1-B4, C5), a soft velocity lid is always present, even if sometimes it is very thin. The cell B4 is characterised by the thinnest lid, and this correlates well with the presence of the Marsili Basin, the youngest seamount in the Southern Tyrrhenian Sea, while the thickest lid occupies a zone (cell A2) where no volcanic activity is known. All the Tyrrhenian submarine volcanic complexes, in cells B1-B4, seem to be fed by the shallow-mantle magma source represented by the very low velocity mantle material present at depths not exceeding 50 km. This is well in agreement with the findings of [78] who assign to the sub-marine volcanic bodies in the Southern Tyrrhenian Sea an extension much larger than previously reported, of about 100 km.

2. *The Aeolian Islands*

The V_s model of these two cells correlates well with the presence, in C5, of Stromboli and, in C4, of Vulcano and Lipari islands.

In spite of their closeness, the V_s distributions versus depth under Stromboli and Vulcano-Lipari are different and a significant difference in the geochemical signatures of the volcanoes is reported by [105]. The clear difference in the V_s distri-

bution, between the eastern (containing Stromboli island) and the central-western (containing Vulcano and Lipari islands) sectors of the arc, could have been masked by a different positioning of the 1°x1° cells, therefore the geochemical data is a strong support for our findings.

The Moho depth and the lid velocity and thickness in correspondence of the Aeolian Islands and Sicily are in good agreement with the results of [2] and [83].

In their model of the Vulcano island magmatic evolution, [135] give indication on the depths at which magma reservoirs appear and suggest the existence of a deep accumulation reservoir, at about 18-21 km, and of a shallow accumulation level in the upper crust, at a depth of 1.5-5.5 km. Petrological and geochemical data of [51] and [52] show that the magma of the volcano has properties that are characteristic of sources located at different depths. It is possible to associate the layer with V_s in the range 3.75-3.95 km/s, just below the Moho, in C4, to the deepest magma reservoir found by [135], while our data resolution does not allow us to sort out the uppermost (crustal) accumulation zone. The presence of a magma reservoir, deeper than about 15 km, possibly correlated with a mantle wedge, is a common feature to all active volcanoes in the area (see triangles in Fig. 1).

3. *The Campanian Province*

Ischia Island (cell A3) and Vesuvius-Phlegraean Fields (cell A4) constitute the Campanian Province [106]. The crust is remarkably different in Ischia and Vesuvio-Phlegraean Fields, while a low V_s (as low as about 3.1 km/s) characterises the uppermost mantle of the whole area.

The V_s distributions versus depth under the Phlegraean Fields and Vesuvius on one side and Stromboli volcano on the other side are remarkably similar, and a recent geochemical investigation [105] reveals close compositional affinities between the Phlegraean Fields, Vesuvius and Stromboli. Thus there seems to be a good correlation between this volcanic activity and the subducting Adriatic (Vesuvius and Phlegraean Fields) and Ionian (Stromboli) slabs proposed by [58]. The main difference between our model and that of [58] is that, under the Vesuvio-Phlegraean Fields, we see a continuous slab and not a broken one and the asthenospheric window is limited to Calabria.

4. *The transitional and continental area*

Continental marginal areas are found at the transition zone between the Tyrrhenian Basin (oceanic structure) and the Calabria region (see Fig. 4) with its Ionian offshore [101], in cells B5-B7. The Tyrrhenian offshore of Sicily (cells C1 and C2) can be classified as continental and, in correspondence of the, now inactive, Pleistocene volcanic island of Ustica (cell C3), there is no evidence of a mantle wedge and the lid velocity increases with depth to as much as 4.65 km/s, as in a

continental-like region. The models obtained in the Ionian area cannot be easily associated to the ones proposed by [87] but, since they miss the high velocity (V_s > 3.6 km/s) lower crust, they can be assimilated to continental margin structures.

5. *The subduction of the Ionian Lithosphere*

Along a section crossing cells C8-C5 it is possible to identify the presence of a high velocity body dipping towards north-west below the Tyrrhenian Sea and a similar body is evidenced by [83]. To focus on such a feature, in Fig. 5 we have plotted the vertical cross-section, extended to 500 km on the base of the distribution of intermediate and deep focus events, of a profile from the Tyrrhenian Sea to the Ionian Sea along the line AB (in the insert). The line AB follows the palaeogeographic prolongation of the Ionian "Ocean" towards the north-west, as proposed by [23]. Since the representation of the solution with its confidence interval is a graphical problem of some complexity, the section AB in Fig. 5 represents a simplified description of the inverse problem results. It gives the velocity and thickness ranges consistent with the observations: the V_s values of likely crustal layers are not indicated (see Tab. 5 for details) and below the depth of 349 km the model parameters are fixed according to [41]; the grey bands in the mantle indicate the range of variability of the layer's thickness and the group of numbers indicate the ranges for V_s in km/s. Clear vertical variation in V_s is detected in most of the cells, with the exception of C7 and D7, where a single mantle layer more than 200 km thick and with average V_s of about 4.4 km/s is also compatible with the inversion results. The dot-dashed and the dashed lines outline the slab and the Moho, respectively. In the upper part of the figure, from west to east the triangles indicate, in the order, the position of the volcanic edifices of Magnaghi, Vavilov, Marsili and Stromboli along the section. The shallow, intermediate-depth and deep events, with the depth error bars, as given in the ISC catalogue, are plotted for the time interval 1964-2000. Owing to the three-dimensionality of the seismogenic body, we plot only the events that fall into a band, about 100 km wide, along the line AB, as shown in the insert.

The main features in Fig. 5 are: the low V_s layers (very shallow asthenosphere) below the thin lid, corresponding to the shallow-mantle magma sources of the huge volcanic bodies in the Tyrrhenian area (Magnaghi-Vavilov and Marsili Basins); the very low velocity layer (mantle wedge) below a thin uppermost lid in the Stromboli area; the stratification in the uppermost upper mantle beneath Calabria, representing a lithospheric doubling (well in agreement with the Moho map compiled by [88], which shows areas with complex crustal structure, where shearing and thrusting involve the whole crust and upper mantle, causing the occurrence of more than one crust-mantle discontinuity); the high velocity body of the Ionian subducting lithosphere towards north-west and below the Southern Tyrrhenian Sea; the two-layers body with V_s in the range 4.35-4.6 km/s (marked by sporadic intermediate-depth seismicity) near the center of the section and above the slab, probably due to

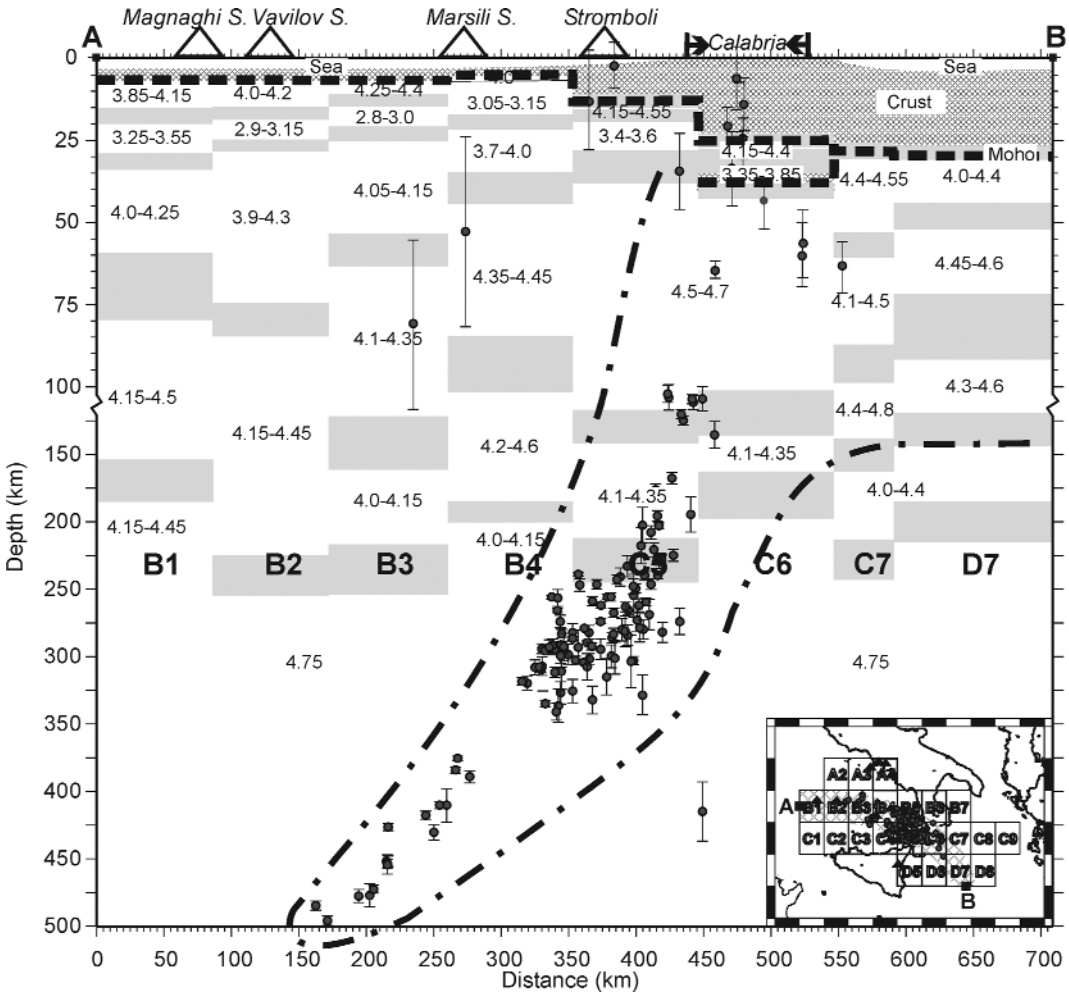

Fig. 5 - Vertical cross-section obtained merging the chosen solutions for the cells B1, B2, B3, B4, C5, C6, C7 and D7 (with balanced horizontal distances) crossed by the section AB (from the Tyrrhenian Sea to the Ionian Sea; see the insert). The section is extended to 500 km only on the basis of the distribution of the intermediate and deep focus events. The V_s values of likely crustal layers are not indicated (see Tab. 2 for the details). In the mantle, the grey bands indicate the boundaries between layers, that can well be transition zones in their own right, and the group of numbers indicate the ranges for V_s in km/s (see Tab. 5). Clear vertical variation in V_s is detected in most of the cells, with the exception of C7 and D7, where a single mantle layer more than 200 km thick and with average V_s about 4.4 km/s is compatible with the inversion results. Below the depth of 349 km the model parameters are fixed according to [41]. The dot-dashed and the dashed lines outline the slab and the Moho, respectively. In the upper part of the figure, from West to East, the triangles delineate the position of the volcanic edifices of Magnaghi-Vavilov, Marsili and Stromboli along the section. In the insert, the location of all the recent volcanoes in the Tyrrhenian area is shown (for more details see caption of Fig. 1). The shallow, intermediate and deep seismicity with the depth error bar, as given in the ISC catalogue, is plotted. The events fall into a band (the shadowed stripe in the insert), about 100 km wide along AB.

the thermal effects induced by the mechanical interaction between the Ionian lithosphere and the hot Tyrrhenian upper mantle [128]. In the center of the section, the layer with V_s in the range 4.0-4.15 km/s and deeper than about 160 km, can be explained by dehydration processes and melting along the down going slab. In fact, the presence of water can significantly alter seismic velocities: formation of even small amounts of free water through the dehydration of hydrous minerals is known to significantly lower seismic velocities in crustal rocks and the water reduces mantle seismic velocities through enhanced an elasticity ([54] and references therein).

In the Ionian area the crustal thickness is less than 30 km and the lithospheric upper mantle is characterised by a relatively soft velocity body (V_s in the range 4.0-4.5 km/s) that lies just below the Moho in D7 and between two faster layers in C7. At depths greater than about 150 km, a low velocity (V_s in the range 4.0-4.4 km/s) asthenospheric layer is present. Further to the west, crossing Calabria, the low velocity asthenospheric layer is absent and the relatively low velocity body in the lithospheric mantle becomes deeper and thicker going towards west. This layering seems to be consistent with the subduction of serpentinized and attenuated continental lithosphere formed in response to the Jurassic extensional phase. In fact, in zones of lithospheric extension, due to either laterally directed horizontal forces and/or an upwelling mantle plume [14], a continental lithosphere starts to reduce its thickness, allowing hot asthenospheric mantle to reach much shallower depths. If the stresses are maintained, a new ocean basin may form as in the Tyrrhenian basin. If the strain rate starts to diminish, the lithosphere approaches its original thickness but with a thinner crust, as could have occurred in the Mesozoic Ionian lithosphere (e.g. cells C7, C8 and D6-D8). During the tensional phase, the relatively low velocity (V_s in the range 4.0-4.5 km/s) layer, that according to [125] seems to extend to the South Adriatic Sea, could be formed as result of the serpentinization of peridotites. Such process produces velocity reductions of a few percent, as shown by the experiments of [26], and a relevant expansion of rocks that could have supplied the uplift required by the palaeodynamic and palaeogeographic review of [11]. The presence of a low velocity layer of chemical and not of thermal origin is consistent with the low heat flow in the Ionian Sea [33]. This layer when subducted gets thicker, consistently with the dehydration of serpentinite, which is responsible of the weakening of the neighbouring material and may reach depths of 150-200 km [121].

Conclusion

The high percentage of partial melting in the upper mantle of the Tyrrhenian Sea produces V_s values that are usually observed only in crustal layers ($V_s < 3.9$ km/s). This fact makes difficult the seismic definition, at cellular level, of the thickness of the crust and consequently of its nature. A clear example is seen in cells C5

and C6, where there is a layer with V_s in the range 3.4-3.6 km/s and 3.35-3.85 km/s, respectively, below a high velocity mantle layer. In cell C5 a detailed analysis of the seismicity leads to two distinct interpretations of this layer (two-faced «Janus»). If we plot only the hypocenters that fall into the band 100 km wide (i.e. of width similar to that of a cell), along the line AB, the «Janus» layer is totally aseismic and therefore it can be reasonably assigned to the mantle, where it may represent the deeper magma source for Stromboli [135]. On the other side, if all the earthquakes falling in the cells crossed by the line AB are plotted, the «Janus» layer is occupied only by hypocenters of events located either in Sicily and Calabria (continental area) or close to their shoreline. In such a case the layer can be reasonably assigned to the brittle crust, thus the lithospheric doubling is not limited to C6 but it can be extended to the continental side of C5. Keeping this in mind, in the interpretation shown in Fig. 6, the particular feature of the lithospheric doubling is unambiguously detected by our data in correspondence of Southern Calabria, and could be present in correspondence of the Northern Calabria area as well.

Our data do not resolve at depths greater than about 250 km, therefore, below this depth the slab is outlined only on the base of the hypocenters distribution of the intermediate-depth and deep seismicity [15, 21]. The seismicity is distributed along the slab and it seems to decrease, but it is not absent, in correspondence of the serpentinized peridotites in the Ionian lithosphere. Acoustic emission measurements during antigorite dehydration [38] indicate that seismicity in the depth range 50-200 km can indeed be generated by dehydration reactions in the subducting slab.

The heat flow values [33, 84] and the mean Bouguer [80] and Airy [13] gravity anomalies correlate well with the lateral variations of the crustal thickness and of the sub-Moho V_s. In particular, the Airy anomaly, about -20 mGal in the Ionian Sea and up to 60 mGal in the Tyrrhenian Sea, reflects the difference in the lithosphere in the two domains. Cell B4 represents the «transition» zone between the very different Ionian and the Tyrrhenian domains. In the studied part of the Ionian Sea, the lithosphere is attenuated continental, thermally relaxed after the Jurassic extensional phase, while in the Southern Tyrrhenian Sea it is very young oceanic.

In Fig. 6 the different patterns are used to identify the main properties in the study area: (1) the asthenospheric low velocity zone in the Tyrrhenian and Ionian areas; (2) the body with relatively high V_s, in the range 4.2-4.6 km/s, above the slab, probably due to the thermal effects induced by the mechanical interaction between the Ionian lithosphere and the hot Tyrrhenian upper mantle; (3) the shallow magma reservoir extending in the whole Tyrrhenian Sea, below a very thin lid, and between the base of the Tyrrhenian plate and the top of the Ionian slab; (4) the low velocity layer within the subducting slab, consistent with the subduction of serpentinized and attenuated continental lithosphere formed in response to the Jurassic extensional phase; (5) the layer with V_s in the range 4.0-4.15 km/s, extending deeper than about 160 km in the centre of the section, consistent with dehydration processes and melting along the down going slab.

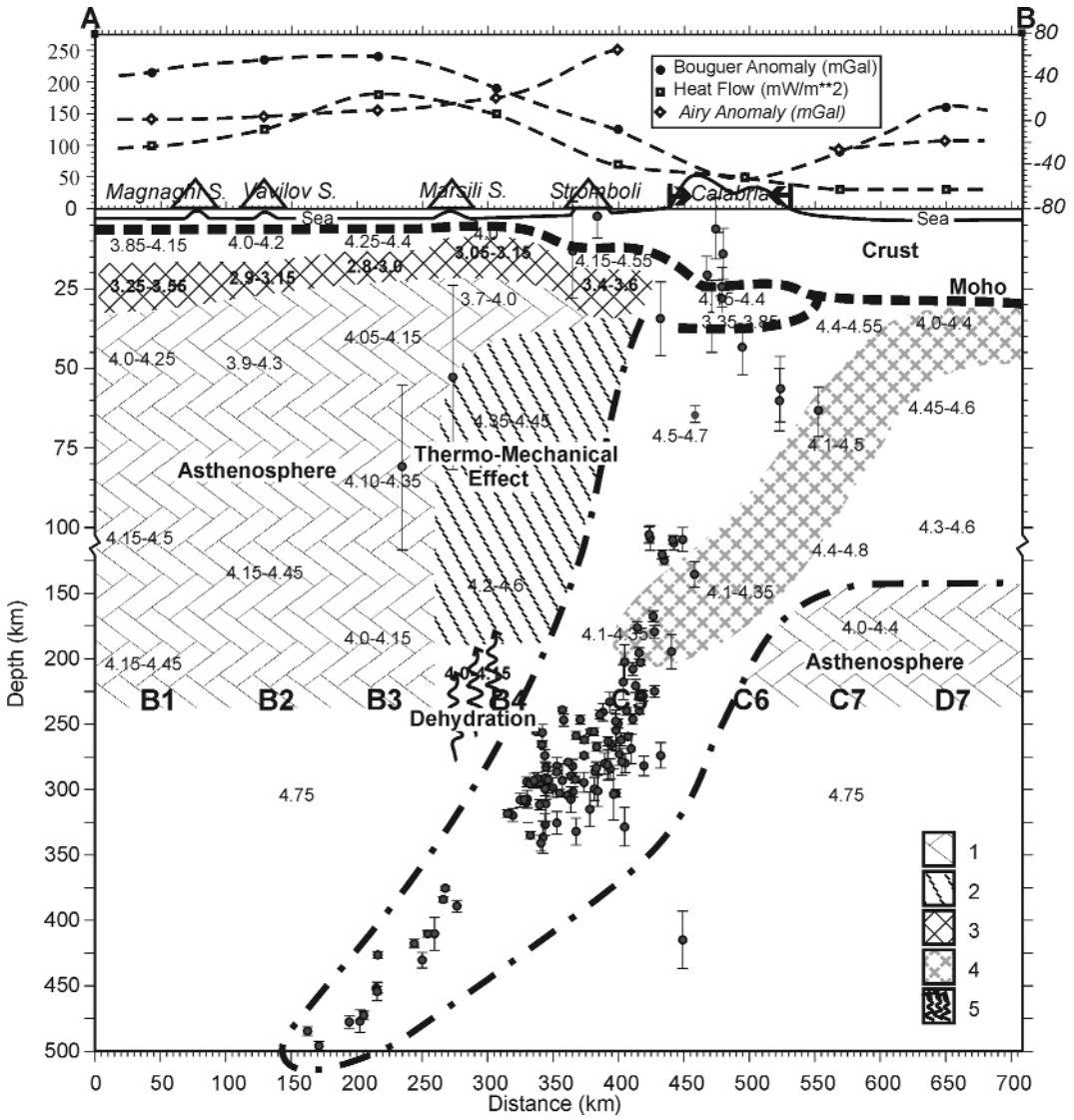

Fig. 6 - Interpretative sketch of section AB of Fig. 5. The dot-dashed and the dashed lines outline the slab and the Moho, respectively. From West to East the triangles delineate the position of the volcanic edifices along the section. The mean values of the heat flow [33, 84], of the Bouguer anomaly [80] and of the Airy anomaly [13] are plotted in the upper part of the figure (the italic scale, on the right, is for the Airy anomaly). The different patterns indicate: (1) the asthenospheric channel in the Tyrrhenian and Ionian areas; (2) the body with V_s about 4.4 km/s above the slab, probably due to the thermal effects induced by the mechanical interaction between the subducting Ionian lithosphere and the hot Tyrrhenian upper mantle; (3) the shallow magma reservoir extending in the whole Tyrrhenian Sea, below a very thin lid, and between the base of the Tyrrhenian plate and the top of the Ionian slab; (4) the low velocity layer within the subducting slab, consistent with the subduction of serpentinized and attenuated continental lithosphere formed in response to the Jurassic extensional phase; (5) the layer with V_s around 4.0 km/s, extending from about 140 km to 220 km of depth in the centre of the section, explained by dehydration processes and melting along the down going slab.

Furthermore, the seismicity in cell B5 is shallower than 25 km and deeper than 240 km, i.e. the asthenospheric layer with V_s in the range 4.05-4.15 km/s is totally aseismic. The V_s structure and the earthquakes distribution in the average depth range from 130 km to 250 km in B5 is consistent with the detachment of the Adriatic slab, surmounted by the lithosphere of the overriding Tyrrhenian Plate, as indicated in the three-dimensional sketch of the Southern Tyrrhenian subduction zone proposed by [58]. The slab detachment, instead, is not seen in our model of cell A4, which contains Vesuvio and Phlegraean Fields, and in the pertinent section of [31]. The layering under the mantle wedge in A4 is consistent with the presence of a continuous subducted lithospheric slab (Adria-Ionian), whose relatively low velocity layer (with V_s in the range 4.0-4.15 km/s), found in the depth range from about 130 to less than 200 km, may have the same origin as in cells C5-C6, i.e. can be a layer of serpentinized peridotites. Therefore, the low velocity layer (V_s in the range 4.05-4.15 km/s) in B5 can be a window on the asthenosphere and, in agreement with [94], we assign the intermediate depth seismicity of the cells C5-C6 and B5-B6 to the Ionian slab, and the deep seismicity in cells A4 to the Adriatic slab. A much more indisputable similarity between the sketch of the south Tyrrhenian subduction zone of [58] and our models is seen in cell D5. In this cell the layer about 20-27 km thick, with a V_s in the range 3.9-4.3 km/s, centred at about 38 km of depth, that can well be the deep magma feeder of Etna volcano, well corresponds to the shallow asthenospheric mantle wedge (or asthenospheric window) between the base of the Tyrrhenian plate and the top of the Ionian slab.

The models shown in Fig. 4 and the interpretative section given in Fig. 6 are consistent with the presence of the asthenospheric window feeding Etna volcano [4, 58] and support the hypothesis, formulated from geochemical investigations [105], that the intraplate material is provided by inflow of asthenospheric mantle into the wedge above the subducting plates (Adriatic and Ionian) either through the lithospheric window of the Adriatic lithosphere and/or from the Tyrrhenian Sea region.

Acknowledgements

We are grateful to, G.V., Dal Piaz, C., Doglioni, M.L. Frezzotti, A., Peccerillo, and S. Sinigoi for their very fruitful comments about the geological, geochemical and petrological aspects of our results. This work has been supported by the projects: CNRC007AF8, MURST-COFIN prot. 9904261312_006 (1999), MURST-COFIN prot. MM04158184_002 (2000), MURST-COFIN prot. 2001045878_007 (2001), INGV project «Eruptive Scenarios from Physical Modeling and Experimental Volcanology».

REFERENCES

[1] Ahrens T.J., 1973. Petrologic properties of the upper 670 km of the Earth's mantle; geophysical implications. *Physics of the Earth and Planetary Interiors*, 7, 167-186.
[2] Alessandrini B., L. Beranzoli, G. Drakatos, C. Falcone, G. Karantonis, F.M. Mele, G.N. Stavrakakis, 1997. Tomographic image of the crust and uppermost mantle in the Ionian and Aegean regions. *Annali di Geofisisica*, XL, 1, 151-160.
[3] Alessandrini B., L. Beranzoli, F.M. Mele, 1995. 3D crustal P-wave velocity tomography of the Italian region using local and regional seismicity data. *Annali di Geofisica*, 38, 2, 189-211.
[4] Anderson H., J. Jackson, 1987. Active tectonics of the Adriatic Region. *Geophysical Journal of the Royal Astronomical Society*, 91, 937-983.
[5] Babuska V., J. Plomerova, 1990. Tomographic studies of the upper mantle beneath the Italian region. *Terra Nova*, 2, 569-576.
[6] Backus G., J.F. Gilbert, 1968. Resolving power of gross earth data. *Geophysical Journal of the Royal Astronomical Society*, 16, 168-205.
[7] Backus G., J.F. Gilbert, 1970. Uniqueness in the inversion of inaccurate gross earth data. *Philosophical Transactions of the Royal Society*, 266, 123-192.
[8] Bijwaard H., W. Spakman, E.R. Engdahl, 1998. Closing the gap between regional and global travel time tomography. *Journal of Geophysical Research*, 103, B12, 30.055-30.078.
[9] Biswas N.N., L. Knopoff, 1974. The structure of the Upper Mantle under the U.S. from the dispersion of Rayleigh waves. *Geophysical Journal of the Royal Astronomical Society*, 36, 515-539.
[10] Bolt B.A., J. Dorman, 1961. Phase and Group velocity of Rayleigh waves in a spherical gravitating earth. *Journal of Geophysical Research*, 66, 2965-2981.
[11] Bosellini A., 2002. Dinosaurs «re-write» the geodynamics of the eastern Mediterranean and the paleogeography of the Apulia Platform. Earth Science Review, 59, 211-234.
[12] Bottinga Y., L . Steinmetz, 1979. A geophysical, geochemical, petrological model of the submarine lithosphere. *Tectonophysics*, 55, 311-347.
[13] Bowin C., W. Warsi, J. Milligan, 1981. *Free-Air gravity anomaly map of the world.* Woods Hole Oceanographic Institution, Woods Hole, Massachussetts 02543, Published by The Geological Society of America.
[14] Brown G.C., A.E. Mussett, 1995. *The inaccessible Earth*. Chapman and Hall, London, 276 pp.
[15] Bruno G., I. Guerra, A. Moretti, G. Neri, 1999. Space variations of stress along the Tyrrhenian Wadati-Benioff zone. *Pure and Applied Geophysics*, 156, 667-688.
[16] Calanchi N., A. Peccerillo, C.A. Tranne, F. Lucchini, P.L. Rossi, P. Kempton, M. Barbieri, T.W. Wu, 2002. Petrology and geochemistry of volcanic rocks from the islands of Panarea: implications for mantle evolution beneath the Aeolian island arc (southern Tyrrhenian sea). *Journal of Vulcanology and Geothermal Research*, 115, 367-395.
[17] Calcagnile G., F. D'Ingeo, P. Farrugia, G.F. Panza, 1982. The lithosphere in the central-eastern Mediterranean area. *Pure and Applied Geophysics*, 120, 389-406.
[18] Calcagnile G., G.F. Panza, 1981. The main characteristics of the Lithosphere-Asthenosphere System in Italy and surrounding regions. *Pure and Applied Geophysics*, 119, 865-879.
[19] Caputo M., G.F. Panza, D. Postpischl, 1970. Deep structure in the Mediterranean Basis. *Journal of Geophysical Research*, 75, 26, 4919-4923.
[20] Caputo M., L. Knopoff, E. Mantovani, S. Mueller, G.F. Panza, 1976. Rayleigh wave phase velocities and upper mantle structure in the Apennines. *Annali di Geofisica*, 29, 199-21.
[21] Caputo M., G.F. Panza, D. Postpischl, 1972. New evidences about the deep structure of the Lipari arc. *Tectonophysics*, 15, 219-231.

[22] Catalano R., P. Di Stefano, A. Sulli, F.P. Vitale, 1996. Paleogeography and structure of the central Mediterranean: Sicily and its offshore area. *Tectonophysics*, 260, 291-323.
[23] Catalano R., C. Doglioni, S. Merlini, 2001. On the Mesozoic Ionian Basin. *Geophysical Journal International*, 144, 49-64.
[24] Cernobori L., A. Hirn, J.H. McBride, R. Nicolich, L. Petronio, M. Romanelli, STREAMERS/PROFILES Working Groups, 1996. Crustal image of the Ionian basin and its Calabrian margin. *Tectonophysics*, 264, 175-189.
[25] Chimera G., A. Aoudia, A. Saraò, G.F. Panza, 2003. Active Tectonics in Central Italy: constraints from surface wave tomography and source moment tensor inversion. *Physics of the Earth and Planetary Interiors*, 138, 241-262.
[26] Christensen N.I., 1966. Elasticity of Ultrabasic Rocks. *Journal of Geophysical Research*, 71, 24, 5921-5931.
[27] Cimini G.B., P. De Gori, 1997. Upper mantle velocity structure beneath Italy from direct and secondary P-wave teleseismic tomography. *Annali di Geofisisica*, XL, 1, 175-194.
[28] Cloetingh S., G. Nolet, R. Wortel, 1980. Crustal structure of the eastern Mediterranean inferred from Rayleigh wave dispersion. *Earth and Planetary Science Letters*, 51, 336-342.
[29] Cristofolini R., F. Ghisetti, R. Scarpa, L. Vezzani, 1985. Character of the stress field in the Calabrian Arc and Southern Apennines (Italy) as deducted by geological, seismological and volcanological information. *Tectonophysics*, 117, 39-58.
[30] De Astis G., L. La Volpe, A. Peccerillo, L. Civetta, 1997. Volcanological and petrological evolution of Vulcano island (Aeolian Arc, southern Tyrrhenian Sea). *Journal of Geophysical Research*, 102, B4, 8021-8050.
[31] De Gori P., G.B. Cimini, C. Chiarabba, G. De Natale, C. Troise, A. Deschamps, 2001. Teleseismic tomography of the Campanian volcanic area and surrounding Apenninic belt. *Journal of Vulcanology and Geothermal Research*, 109, 55-75.
[32] deGroot-Hedlin C., S. Constable, 1990. Occam's inversion to generate smooth, two-dimensional models from magnetotelluric data. *Geophysics*, 55, 1613-1624.
[33] Della Vedova B., I. Marson, G.F. Panza, P. Suhadolc, 1991. Upper mantle properties of the Tuscan-Tyrrhenian area: a framework for its recent tectonic evolution. *Tectonophysics*, 195, 311-318.
[34] Della Vedova B., G. Pellis, E. Pinna, 1989. Studio geofisico dell'area di transizione tra il Mar Pelagico e la piana abissale dello Ionio. *Atti 8° Convegno Annuale G.N.G.T.S.*, Roma, 543-558.
[35] De Matteis R., D. Latorre, A. Zollo, J. Virieux, 2000. 1D P-velocity models of Mt. Vesuvio Volcano from the Inversion of TomoVes96 first arrival time data. *Pure and Applied Geophysics*, 157, 1643-1661.
[36] De Voogd B., C. Truffert, N. Chamot-Rooke, P. Huchon, S. Lallermant, X. Le Pichon, 1992. Two-ship deep seismic soundings in the basins of the Eastern Mediterranean Sea (Pasiphae cruise). *Geophysical Journal International*, 109, 536-552.
[37] Ditmar P.G., T.B. Yanovskaya, 1987. A generalization of the Backus-Gilbert method for estimation of lateral variations of surface wave velocity. *Izvestiya, Physics of Solid Earth* (English Translation), 23, 6, 470-477.
[38] Dobson D.P., P.G. Meredith, S.A. Boon, 2002. Simulation of subduction zone seismicity by dehydration of serpentine. *Science*, 298, 1407-1410.
[39] Doglioni C., F. Innocenti, G. Mariotti, 1998. On the geodynamic origin of Mt. Etna. *Proceedings XVII Convegno Gruppo Nazionale Geofisica Terra Solida*, Roma, 1133-1145.
[40] Doglioni C., F. Innocenti, G. Mariotti, 2001. Why Mt. Etna? *Terra Nova*, 13, 25-31.
[41] Du, Z.J., Michelini, A., Panza, G.F., 1998. EurID: a regionalised 3-D seismological model of Europe. *Physics of the Earth and Planetary Interiors*, 105, 31-62.

[42] Du Z.J., G.F. Panza, 1999. Amplitude and phase differentiation of synthetic seismograms: a must for waveform inversion at regional scale. *Geophysical Journal International*, 136, 83-98.
[43] Faccenna C., F. Funiciello, D. Giardini, P. Lucente, 2001. Episodic back-arc extension during restricted mantle convection in the Central Mediterranean. *Earth and Planetary Science Letters*, 187, 105-116.
[44] Farrugia P., G.F. Panza, 1981. Continental character of the lithosphere beneath the Ionian Sea. In: *The solution of the inverse problem in geophysical interpretation*, (R.Cassinis, ed.), Plenum Pub. Corp., 327-334.
[45] Ferrucci F., G. Gaudiosi, A. Hirn, R. Nicolich, 1991. Ionian Basin and Calabrian Arc: some new elements from DSS data. *Tectonophysics*, 195, 411-419.
[46] Finetti I., 1982. Structure, stratigraphy and evolution of central Mediterranean. *Bollettino di Geofisica Teorica e Applicata*, 24, 96.
[47] Finetti I.R., M. Boccaletti, M. Bonini, A. Del Ben, R. Geletti, M. Pipan, F. Sani, 2001. Crustal section based on CROP seismic data across the North Tyrrhenian - Northern Apennines - Adriatic Sea. *Tectonophysics*, 343, 135-163.
[48] Finetti I.R., A. Del Ben, 1986. Geophysical study of the Tyrrhenian opening. *Bollettino di Geofisica Teorica e Applicata*, 28, 110, 75-156.
[49] Finetti I.R., F. Lentini, S. Carbone, S. Catalano, A. Del Ben, 1996. Il sistema Appennino Meridionale-Arco Calabro-Sicilia nel Mediterraneo Centrale: studio geologico-geofisico. *Bollettino della società geologica italiana*, 115, 529-559.
[50] Fowler C.M.R., 1995. *The Solid Earth. An introduction to Global Geophysics*. Cambridge Univ. Press.
[51] Francalanci L., S. Tommasini, S. Conticelli, G.R. Davies, 1999. Sr isotope evidence for short magma residence time for the 20th century activity at Stromboli volcano, Italy. *Earth and Planetary Science Letters*, 167, 1-2, 61-69.
[52] Gauthier P.J., M. Condomines, 1999. ^{210}Pb–^{226}Ra radioactive disequilibria in recent lavas and radon degassing: inferences on the magma chamber dynamics at Stromboli and Merapi volcanoes. *Earth and Planetary Science Letters*, 172, 1-2, 111-126.
[53] Gobarenko V.S., S.B. Nikolova, S.J. Sokolova, 1990. Velocity structure of the western Mediterranean from inversion of P-wave traveltimes. *Geophysical Journal International*, 101, 557-564.
[54] Goes S., R. Govers, P. Vacher, 2000. Shallow mantle temperatures under Europe from P and S wave tomography. *Journal of Geophysical Research*, 105, B5, 11.153-11.169.
[55] Graham E.K., 1970. Elasticity and composition of the upper mantle. *Geophysical Journal of the Royal Astronomical Society*, 20, 285-302.
[56] Gueguen E., C. Doglioni, M. Fernandez, 1997. Lithospheric boudinage in the Western Mediterranean back-arc basin. *Terra Nova*, 9, 184-187.
[57] Gutenberg B., C.F. Richter, 1956. Earthquake magnitude, intensity, energy and acceleration. *Bulletin of the Seismological Society of America*, 46, 105-145.
[58] Gvirtzman Z., A. Nur, 1999. The formation of Mount Etna as the consequence of slab rollback. *Nature*, 401, 782-785.
[59] Hazler S.E., A.F. Sheehan, D.E. McNamara, W.R. Walter, 2001. One-dimensional shear velocity structure of Northern Africa from Rayleigh wave group velocity dispersion. *Pure and Applied Geophysics*, 158, 1475-1493.
[60] Herak M., G.F. Panza. G. Costa, 2001. Theoretical and observed depth correction for M_s. *Pure and Applied Geophysics*, 158, 1517-1530.
[61] ISC. International Seismological Centre On-line Bulletin, 2001. http://www.isc.ac.uk/Bull, International Seismological Centre, Thatcham, United Kingdom.
[62] Ismail-Zadeh A.T., R. Nicolich, L. Cernobori, 1998. Modelling of geodynamic evolution of the Ionian Sea basin. *Computational Seismology and Geodynamics*, 30, 32-50.

[63] Karagianni E.E., D.G. Panagiotopoulos, G.F. Panza, P. Suhadolc, C.B. Papazachos, B.C. Papazachos, A. Kiratzi, D. Hatzfeld, K. Makropoulos, K. Priestley, A. Vuan, 2002. Rayleigh Wave Group Velocity Tomography in the Aegean area. *Tectonophysics*, 358, 187-209.
[64] Kasten K.A., J. Mascle, O.L.S. Party, 1988. ODP Leg 107 in the Tyrrhenian Sea: insights into passive margin and backarc basin evolution. *Geological Society of America Bulletin*, 100, 1140-1156.
[65] Keith M., 2001. Evidence for a plate tectonics debate. *Earth-Science Reviews*, 55, 235-336.
[66] Kern H., V. Schenk, 1988. A model of velocity structure beneath Calabria, southern Italy, based on laboratory data. *Earth and Planetary Science Letters*, 87, 325-337.
[67] Knopoff L., 1972. Observations and inversion of surface-wave dispersion. *Tectonophysics*, 13, 497-519.
[68] Knopoff L., G.F. Panza, 1977. Resolution of Upper Mantle Structure using higher modes of Rayleigh waves. *Annales Geophysicae*, 30, 491-505.
[69] Knox R.P., A.A. Nyblade, C.A. Langston, 1998. Upper mantle S velocities beneath Afar and western Saudi Arabia from Rayleigh wave dispersion. *Geophysical Research Letters*, 25, 22, 4233-4236.
[70] Levshin A.L., V.F. Pisarenko, G.A. Pogrebinsky, 1972. On a frequency time analysis of oscillations. *Annales Geophysicae*, 28, 211-218.
[71] Levshin A.L., L. Ratnikova, J. Berger, 1992. Peculiarities of surface wave propagation across Central Eurasia. *Bulletin of the Seismological Society of America*, 82, 2464-2493.
[72] Lliboutry L., 2000. *Quantitative geophysics and geology*. Springer ed., Praxis Publ., Chichester, UK.
[73] Locardi E., 1986. Tyrrhenian volcanic arcs: volcano-tectonics, petrogenesis and economic aspects. In: *The origin of the arcs* (F.C. Wezel, ed.), Elsevier, 351-373 pp.
[74] Lucente F.P., C. Chiarabba, G.B. Cimini, D. Giardini, 1999. Tomographic constraints on the geodynamic evolution of the Italian region. *Journal of Geophysical Research*, 104, B9, 20.307-20.327.
[75] Makris J., 1981. Deep structure of the Eastern Mediterranean deduced from refraction seismic data. In: *Sedimentary basins of Mediterranean margins* (F.C. Wezel ed.), Tecnoprint Bologna, 63-64 pp.
[76] Makris J., A. Ginzburg, 1987. The Afar depression: transition between continental rifting and sea-floor spreading. *Tectonophysics*, 141, 199-214.
[77] Mantovani E., G. Nolet, G.F. Panza, 1985. Lateral heterogeneity in the crust of the Italian region from regionalized Rayleigh-wave group velocities. *Annales Geophysicae*, 3, 519-530.
[78] Marani M.P., T. Trua, 2002. Thermal constriction and slab tearing at the origin of a super-inflated spreading ridge: the Marsili Volcano (Tyrrhenian Sea). *Journal of Geophysical Research*, 107, B9, 2188.
[79] Marquering H., R. Snieder, 1996. Shear-wave velocity structure beneath Europe, the north-eastern Atlantic and western Asia from waveform inversion including surface-wave mode coupling. *Geophysical Journal International*, 127, 283-304.
[80] Marson I., G.F. Panza, P. Suhadolc, 1995. Crust and upper mantle models along the active Tyrrhenian rim. *Terra Nova*, 7, 348-357.
[81] Martinez M.D., J.A. Canas, X. Lana, J. Badal, 2001. Objective regionalization of Rayleigh wave dispersion data by clustering algorithms: an application to the Mediterranean basin. *Tectonophysics*, 330, 245-266.
[82] Martinez M.D., X. Lana, J. Badal, J.A. Canas, L. Pujades, 1997. Preliminary objective regionalization of the Mediterranean basin derived from surface-wave tomography. *Annali di Geofisisica*, XL, 1, 43-59.
[83] Martinez M.D., X. Lana, J.A. Canas, J. Badal, L. Pujades, 2000. Shear-wave velocity tomography of the lithosphere-asthenosphere system beneath the Mediterranean area. *Physics of the Earth and Planetary Interiors*, 122, 33-54.

[84] Mongelli F., G. Zito, G. Castaldi, R. Celati, B. Della Vedova, B. Fanelli, M. Nuti, G. Pellis, P. Squarci, L. Taffi, 1991. Geothermal regime of Italy and surrounding seas. In: *Terrestrial heat flow and the lithosphere structure* (V. Cermak, L. Rybac, ed.), Springer-Verlag, Berlin Heidelberg.

[85] Morelli C., 1998. Lithospheric structure and geodynamics of the Italian peninsula derived from geophysical data: a review. *Memorie della Società Geologica Italiana*, 52, 113-122.

[86] Mostaanpour M.M., 1984. *Einheitliche Auswertung krustenseismicher Daten in Westeuropa, Darstellung von Krustenparametern und Laufzeitanomalien*. Verlag von Dietrich Reimer in Berlin.

[87] Mueller S., 1978. The evolution of the Earth Crust. In: *Tectonics and Geophysics of Continental Rifts* (I.B. Ramberg, E.R. Neuman, ed.), Reidel, Dordrecht, 11-28 pp.

[88] Nicolich R., R. Dal Piaz, 1990. Moho isobaths. In: *Structural model of Italy and Gravity Map*. Sheet2, Consiglio Nazionale delle Ricerche.

[89] Panza G.F., 1980. Evolution of the Earth's lithosphere. NATO Adv. Stud. Inst. Newcastle, 1979. In: *Mechanisms of Continental Drift and Plate Tectonics* (P.A. Davies, S.K. Runcorn, ed.), Academic Press, 75-87 pp.

[90] Panza G.F., 1981. The resolving power of seismic surface waves with respect to crust and upper mantle structural models. In: *The solution of the inverse problem in geophysical interpretation* (R. Cassinis, ed.), Plenum Publ. Corp., 39-77 pp.

[91] Panza G.F., 1984. Contributi geofisici alla geologia: stato attuale dell'arte e prospettive future. In: *Cento anni di geologia italiana*, Vol. giub. I Centenario S.G.I., Bologna, 363-376 pp.

[92] Panza G.F., G. Calcagnile, 1979. The upper mantle structure in Balearic and Tyrrhenian bathyal plains and the messinian salinity crisis. *Palaeogeo. Palaeoclim. Palaeoeco.*, 29, 3-14.

[93] Panza G.F., G. Calcagnile, P. Scandone, S. Mueller, 1980. La struttura profonda dell'area mediterranea. *Le Scienze*, 141, 60-69.

[94] Panza G.F, F. Romanelli, 2001. Beno Gutenberg contribution to seismic hazard assessment and recent progress in the European-Mediterranean region. *Earth-Science Reviews*, 55, 165-180.

[95] Papazachos B.C., P.E. Comninakis, 1978. Deep structure and tectonics of the Eastern Mediterranean. *Tectonophysics*, 46, 285-296.

[96] Papazachos C.B., P.M. Hatzidimitriou, D.G. Panagiotopoulos, G.N. Tsokas, 1995. Tomography of the crust and upper mantle in southeast Europe. *Journal of Geophysical Research*, 100, B7, 12405-12422.

[97] Papazachos C.B., A.A. Kiratzi, 1996. A detailed study of the active crustal deformation in the Aegean and surrounding area. *Tectonophysics*, 253, 129-153.

[98] Parolai S., D. Spallarossa, C. Eva, 1997. Bootstrap inversion for P_n wave velocity in North-Western Italy. *Annali di Geofisica*, XL, 1, 133-150.

[99] Pasquale V., C. Cabella, M. Verdoya, 1990. Deep temperatures and lithospheric thickness along the European Geotraverse. *Tectonophysics*, 176, 1-11.

[100] Pasquale V., M. Verdoya, P. Chiozzi, 1999. Thermal state and deep earthquakes in the Southern Tyrrhenian. *Tectonophysics*, 306, 435-448.

[101] Pasquale V., M. Verdoya, P. Chiozzi, 2003. Heat-flux budget in the south-eastern continental margin of the Tyrrhenian basin. *Physics and Chemistry of the Earth*, 28, 407-420.

[102] Pasyanos M.E., W.R. Walter, S.E. Hazler, 2001. A surface wave dispersion study of the Middle East and North Africa for Monitoring the Comprehensive Nuclear-Test-Ban Treaty. *Pure and Applied Geophysics*, 158, 1445-1474.

[103] Payo G., 1967. Crustal structure of the Mediterranean Sea by surface waves. Part I: Group Velocity. *Bulletin of the Seismological Society of America*, 57, 2, 151-172.

[104] Payo G., 1969. Crustal structure of the Mediterranean Sea by surface waves. Part II: Phase Velocity and Travel Times. *Bulletin of the Seismological Society of America*, 59, 1, 23-42.

[105] Peccerillo A., 2001. Geochemical similarities between the Vesuvius, Phlegraean Fields and Stromboli Volcanoes: petrogenetic, geodynamic and volcanological implications. *Mineralogy and Petrology*, 73, 93-105.
[106] Peccerillo A., G.F. Panza, 1999. Upper mantle domains beneath central-southern Italy: petrological, geochemical and geophysical constraints. *Pure and Applied Geophysics*, 156, 421-443.
[107] Peishan C., C. Haitong, 1989. Scaling law and its applications to earthquake statistical relations. *Tectonophysics*, 166, 53-72
[108] Pepe F., G. Bertotti, F. Cella, E. Marsella, 2000. Rifted margin formation in the south Tyrrhenian Sea: a high-resolution seismic profile across the north Sicily passive continental margin. *Tectonics*, 19, 2, 241-257.
[109] Piromallo C., A. Morelli, 1997. Imaging the Mediterranean upper mantle by P-wave travel time tomography. *Annali di Geofisica*, 40, 4, 963-979.
[110] Plomerova J., 1997. Seismic anisotropy in tomographic studies of the upper mantle beneath southern Europe. *Annali di Geofisica*, XL, 1, 111-121.
[111] Pontevivo A., G.F. Panza, 2002. Group Velocity Tomography and Regionalization in Italy and bordering areas. *Physics of the Earth and Planetary Interiors*, 134, 1-15.
[112] Ringwood A.E., 1966. Mineralogy of the mantle. In: *Advances in Earth Science* (P.M. Hurley, ed.), MIT Press, 357-399 pp.
[113] Ritzwoller M.H., A.L. Levshin, 1998. Eurasian surface wave tomography: Group velocities. *Journal of Geophysical Research*, 103, B3, 4839-4878.
[114] Russell, B., 1946. *History of western philosophy*. George Allen and Unwind, Ltd.
[115] Scarascia S., A. Lozej, R. Cassinis, 1994. Crustal structures of the Ligurian, Tyrrhenian and Ionian Seas and adjacent onshore areas interpreted from wide-angle seismic profiles. *Bollettino di Geofisica Teorica e Applicata*, 36, 141-144.
[116] Shapiro N.M., M.H. Ritzwoller, 2002. Monte-Carlo inversion for a global shear-velocity model of the crust and upper mantle. *Geophysical Journal International*, 151, 88-105.
[117] Snieder R., 1988. Large scale waveform inversions of surface waves for lateral heterogeneity 2. Application to surface waves in Europe and the Mediterranean. *Journal of Geophysical Research*, 93, B10, 12067-12080.
[118] Spakman W., 1990. Tomographic images of the upper mantle below central Europe and the Mediterranean. *Terra Nova*, 2, 542-553.
[119] Stampfli G.M., J. Mosar, D. Marquer, R. Marchant, T. Baudin, G. Borel, 1998. Subduction and obduction processes in the Swiss Alps. *Tectonophysics*, 296, 159-204.
[120] Trua T., G. Serri, M.P. Marani, A. Renzulli, F. Gamberi, 2002. Volcanological and petrological evolution of Marsili Seamount (Southern Tyrrhenian Sea). *Journal of Volcanology and Geothermal Research*, 114, 441-464.
[121] Ulmer P., V. Trommsdorff, 1995. Serpentine stability to mantle depths and subduction related magmatism. *Science*, 268, 858-861.
[122] Urban L., A. Cichowicz, F. Vaccari, 1993. Computation of analytical partial derivatives of phase and group velocities for Rayleigh waves respect to structural parameters. *Studia Geophysica et Geodaetica*, 36, 14-36.
[123] Valyus V.P., 1972. Determining seismic profiles from a set of observations. In: *Computational Seismology* (V.I. Keilis-Borok, ed.), Consult. Bureau, New-York, 114-118 pp.
[124] Valyus V.P., V.I. Keilis-Borok, A. Levshin, 1969. Determination of the upper-mantle velocity cross-section for Europe. *Proceedings of the Academy of Sciences of the USSR*, 185, 3.
[125] Venisti N., G. Calcagnile, A. Pontevivo, G.F. Panza, 2004. Tomographic study of the Adriatic plate. In print *Pure and Applied Geophysics*.
[126] Vuan A., M. Russi, G.F. Panza, 2000. Group velocity tomography in the Subantartic Scotia Sea region. *Pure and Applied Geophysics*, 157, 1337-1357.

[127] Weigel W., 1978. A tectonic model of the Northern Ionian Sea from Refraction seismic data In: *Alps, Apennines, Hellenides* (H. Closs, D. Roeder, K. Schmidt, ed.), Schweizerbart'sche, Stuttgart, 328-329 pp.

[128] Willet S.D., D.C. Pope, 2004. Thermo-Mechanical models of convergent orogenesis: thermal and rheologic dependence of crustal deformation. In: *Rheology and deformation of the lithosphere at continental margins* (G.D. Karnel, B. Taylor, N.W. Driscoll, D.L. Kohlstedt, ed.), Columbia University Press, New York.

[129] Yanovskaya T.B., 1984. Solution of the inverse problem of seismology for laterally inhomogeneous media. *Geophysical Journal of the Royal Astronomical Society*, 79, 293-304.

[130] Yanovskaya T.B., L.M. Antonova, 2000. Lateral variations in the structure of the crust and upper mantle in the Asian region from data on the group velocities of Rayleigh waves. *Izvestiya, Physics of Solid Earth* (English Translation), 36, 2, 121-128.

[131] Yanovskaya T.B., L.M. Antonova, V.M. Kozhevnikov, 2000. Lateral variations of the upper mantle structure in Eurasia from group velocities of surface waves. *Physics of the Earth and Planetary Interiors*, 122, 19-32.

[132] Yanovskaya T.B., P.G. Ditmar, 1990. Smoothness criteria in surface-wave tomography. *Geophysical Journal International*, 102, 63-72.

[133] Yanovskaya T.B., E.S. Kizima, L.M. Antonova, 1998. Structure of the crust in the Black Sea and adjoining regions from surface wave data. *Journal of Seismology*, 2, 303-316.

[134] Yanovskaya T.B., R. Maaz, P.G. Ditmar, H. Neunhofer, 1988. A method for joint interpretation of the phase and group surface-wave velocities to estimate lateral variations of the Earth's structure. *Physics of the Earth and Planetary Interiors*, 51, 59-67.

[135] Zanon V., M. Frezzotti, A., Peccerillo, 2003. Magmatic feeding system and crustal magma accumulation beneath Vulcano Island (Italy): evidence from CO_2 fluid inclusions in quartz xenoliths. *Journal of Geophysical Research*, 108, B6, 2298.

[136] Zhang Y., T. Tanimoto, 1992. Ridges, hotspots and their interaction as observed in seismic velocity maps. *Nature*, 355, 45-49.

[137] Zito, G., Mongelli, F., de Lorenzo, S., Doglioni, C., 2003. Heat flow and geodynamics in the Tyrrhenian Sea. *Terra Nova*, 15, 425-432.